5-18-2016

Tidal River Dynamics: Implications for Deltas

Ton Hoitink
Wageningen University

David A. Jay
Portland State University

Citation Details

Hoitink, A. J. F., & Jay, D. A. (2016). Tidal river dynamics: Implications for deltas. Reviews of Geophysics, 54(1), 240–272. http://doi.org/10.1002/2015RG000507

AGU PUBLICATIONS

Reviews of Geophysics

REVIEW ARTICLE
10.1002/2015RG000507

Key Points:
- Tidal rivers are a vital and little studied nexus between physical oceanography and hydrology
- Signal processing techniques and mechanistic understanding of tidal rivers address the research gap
- River-tide interactions impact delta deposits, channel bifurcation, avulsion, and salt intrusion

Correspondence to:
A. J. F. Hoitink,
ton.hoitink@wur.nl

Citation:
Hoitink, A. J. F., and D. A. Jay (2016), Tidal river dynamics: Implications for deltas, *Rev. Geophys.*, *54*, 240–272, doi:10.1002/2015RG000507.

Received 15 OCT 2015
Accepted 26 FEB 2016
Accepted article online 29 FEB 2016
Published online 31 MAR 2016
Corrected 18 MAY 2016

The copyright line for this article was changed on 18 MAY 2016 after original online publication.

Tidal river dynamics: Implications for deltas

A. J. F. Hoitink[1] and D. A. Jay[2]

[1]Hydrology and Quantitative Water Management Group, Department of Environmental Sciences, Wageningen University, Wageningen, Netherlands, [2]Department of Civil and Environmental Engineering, Portland State University, Portland, Oregon, USA

Abstract Tidal rivers are a vital and little studied nexus between physical oceanography and hydrology. It is only in the last few decades that substantial research efforts have been focused on the interactions of river discharge with tidal waves and storm surges into regions beyond the limit of salinity intrusion, a realm that can extend inland hundreds of kilometers. One key phenomenon resulting from this interaction is the emergence of large fortnightly tides, which are forced long waves with amplitudes that may increase beyond the point where astronomical tides have become extinct. These can be larger than the linear tide itself at more landward locations, and they greatly influence tidal river water levels and wetland inundation. Exploration of the spectral redistribution and attenuation of tidal energy in rivers has led to new appreciation of a wide range of consequences for fluvial and coastal sedimentology, delta evolution, wetland conservation, and salinity intrusion under the influence of sea level rise and delta subsidence. Modern research aims at unifying traditional harmonic tidal analysis, nonparametric regression techniques, and the existing understanding of tidal hydrodynamics to better predict and model tidal river dynamics both in single-thread channels and in branching channel networks. In this context, this review summarizes results from field observations and modeling studies set in tidal river environments as diverse as the Amazon in Brazil, the Columbia, Fraser and Saint Lawrence in North America, the Yangtze and Pearl in China, and the Berau and Mahakam in Indonesia. A description of state-of-the-art methods for a comprehensive analysis of water levels, wave propagation, discharges, and inundation extent in tidal rivers is provided. Implications for lowland river deltas are also discussed in terms of sedimentary deposits, channel bifurcation, avulsion, and salinity intrusion, addressing contemporary research challenges.

1. Introduction

Geophysical flows at the Earth's surface in coastal lowlands are primarily governed by river discharge and forcing conditions imposed by the coastal ocean, which we can characterize for present purposes in terms of a complex spectrum of long waves. River discharge is typically studied as a component in the hydrological cycle, responding to catchment hydrological processes that feed the river through multiple tributary channels ("tributaries") and to hydrogeological flows in the subsurface feeding or draining the river. The coastal ocean sets the downstream boundary of a river, causing river dynamics to be influenced by mean sea level (MSL) variations (on timescales of weeks to centuries), tides, tsunamis, and weather-related coastal processes such as storm surges. These coastal processes are typically studied by the discipline of physical oceanography, with links to hydrology, climate studies, and geology. However, physical oceanographers typically limit their scope to the waters seaward of the maximum limit of salinity intrusion, while hydrologists consider the landward limit of tidal water level fluctuations as the downstream boundary in their water balance models. Between the landward limit of salinity intrusion and the tidal intrusion limit, there exists a lowland region ("the tidal river") impacted by tides, surges, and mean sea level variation that has long received comparatively little attention from the geophysical community. The term "tidal river" even lacks a precise boundary.

The section of a river impacted by tides and other marine forcing processes but void of salinity can be referred to as a "tidal freshwater river," a "tidal river reach," or simply as a tidal river. Reaches seaward of the tidal river are mostly brackish and are commonly referred to as an estuary. The tidal river may extend hundreds of kilometers inland; in large rivers it is often more extensive (in length and sometimes in area) than the estuary. The above definitions employ salinity as means to define the estuarine landward boundary, following the physics-based literature [e.g., *Dyer*, 1997], which is markedly different from the biological perspective

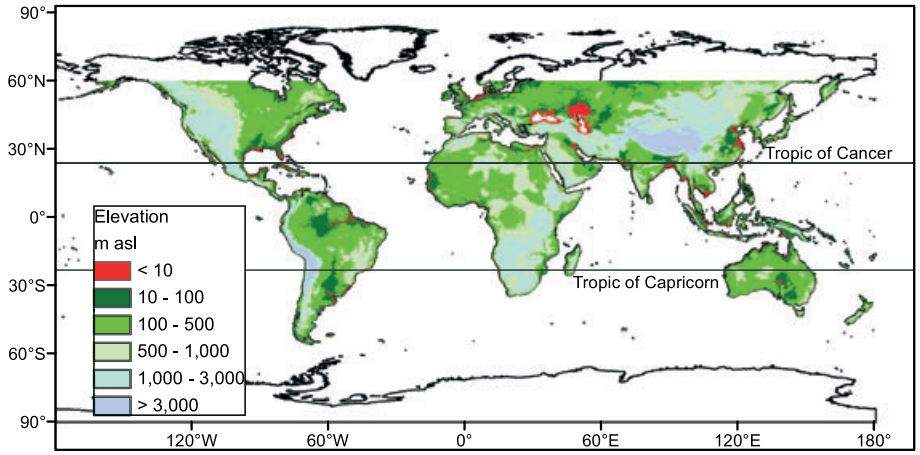

Figure 1. World map of elevation from the Shuttle Radar Topographic Mission (SRTM; data source: CGIAR-CSI), adopted from *Hidayat* [2013]. In regions with elevations less than 10 m, inland rivers are likely to be affected by tidal influences.

[*Elliott and McLusky*, 2002], which tends to include the tidal freshwater reaches in the estuary [e.g., *Day et al.*, 1989]. We offer below a definition of tidal river based on a contemporary understanding of the tidal physics in such systems.

Figure 1 represents elevation of the continents, highlighting the regions with elevation below 10 m (adopted from *Hidayat* [2013]). These tidal river regions influenced by oceanic processes are vast enough to be seen on the global map. One coastal lowland region that stands out in terms of reaching the inner part of a continent is the Amazon depression, which has the largest freshwater runoff of any river basin on Earth [*Milliman and Farnsworth*, 2011]. The outflow from the Amazon is so large that there is no salinity intrusion into its delta, and the Amazon salinity front is found approximately 150 km seaward of the river mouth [*Geyer and Kineke*, 1995]. Still, the landward limit of tidally reversing currents is about 200 km inland [*Uncles et al.*, 2002], and the tidal motion may propagate over a 1000 km into the Amazon depression during low-flow periods [*Kosuth et al.*, 2009]. A similar scenario holds for the third longest river of the world, the Yangtze, where tides propagate as much as 630 km inland [*Zhang et al.*, 2012a]. The Amazon and the Yangtze prove high river discharges can be overwhelmed by even larger tidal discharge amplitudes in the sense that the tide propagates far landward of salinity intrusion and tidal current reversal. That this is an active propagation, not a passive (hydrostatic) reaction to water level changes at the coast is emphasized by the fact that tidal low-water levels at landward locations may be well above tidal high water levels at the ocean boundary [e.g., *Gallo and Vinzon*, 2005; *Guo et al.*, 2015; *Jay et al.*, 2016].

The interest in tidal freshwater rivers has recently grown in a community that is primarily focused on the world's wetlands. *Barendregt and Swarth* [2013] argue that river ecologists have long avoided the extremely complex regions where rivers experience tidal fluctuations. This may relate to their disciplinary background, which typically excludes knowledge about tidal physics. Such knowledge is needed to plan field work and define the physics-biology links relevant for ecosystem functioning. Estuarine ecologists, in turn, consider the tidal freshwater zone to be a region outside their scope of interest. Hence, also in ecology, the tidal river represents a realm that has long been left underexplored. *Ensign et al.* [2012] identify a knowledge gap in scientists' understanding of the geomorphic and biogeochemical response of tidal freshwater rivers to sea level rise, climate change, and anthropogenically driven variations in watershed exports. In this context, they formulate contemporary challenges in tidal river research in the form of three questions: (1) how do tidal rivers affect the fluxes of carbon, nitrogen, and phosphorus? (2) how is tidal river morphology affected by sea level rise and climate change influence? and (3) how do those geomorphologic changes affect ecosystem functions that are important to human, wildlife, and plant communities? Results from *Ensign et al.* [2012, 2013, 2014a, 2014b] stress the scarcity of relevant data and the limitations of numerical models for predicting changes in tidal river hydrology and geomorphology, but the long-wave propagation processes that are of primary

interest here also remain poorly understood. Thus, new knowledge about tidal rivers is needed to support progress in wetland restoration, which heavily relies on understanding of both physical and ecological processes [*Jay et al.*, 2015].

Another reason for an increased recent interest in tidal freshwater rivers is the alarming flood vulnerability of river deltas. *Syvitski et al.* [2009] have emphasized the special vulnerability of deltas to MSL rise by focusing on the added effect of deltaic subsidence. The latter occurs as a result of sediment compaction from the removal of oil, gas, and water from the deltas underlying sediments, the trapping of sediment in reservoirs upstream, and floodplain engineering [*Syvitski et al.*, 2009]. These developments not only exacerbate problems of flood vulnerability but also limit freshwater availability due to enhanced salinity intrusion [*Zhang et al.*, 2012b], both of which are directly dependent on the interaction of tides with the river discharge. Because of the strongly nonlinear behavior of tidal hydrodynamics [*Parker*, 1991a], relative MSL rise in deltas does not directly translate, even with constant morphology, into a uniform rise in extreme sea levels [*Vellinga et al.*, 2014]. Moreover, human influences on channel morphology are often overwhelming, greatly altering the interaction of tides, storm surges, and river flood waves. Based on a 50 year database of 18 stations, *Zhang et al.* [2009] found, for example, that water levels in the landward part of the Pearl River Delta show a decreasing trend, while water levels in the middle and lower part show an increasing trend. A similar conclusion applies to the Rhine-Meuse Delta; *Vellinga et al.* [2014] found, based on a 70 year database from 13 stations, that although the annual mean water levels rise at the same pace as the mean sea level, the high water and low water yearly extremes generally decrease. Both *Zhang et al.* [2009] and *Vellinga et al.* [2014] attribute much of these changes to channel deepening for shipping, yet understanding the underlying physical mechanisms requires a better understanding of long-wave propagation in branching tidal rivers.

Here we review existing and ongoing studies that focus on the physics of long-wave propagation in tidal rivers and discuss implications for sedimentary deposits, channel bifurcation, avulsion, and salinity intrusion. We start in section 2 by describing the most distinctive phenomena observed in tidal freshwater rivers. We synthesize existing insights from analytical models and discuss alternative definitions that apply to tidal rivers. We then present a comprehensive overview of techniques for time series analysis of tidal river dynamics in section 3, including a procedure that can be used to select an appropriate method of analysis. Section 4 discusses the physics of river discharge-tide interactions and techniques to remove the tide from a discharge series and explains how river discharge can be inferred from tidal properties. In section 5, implications of river discharge-tide interactions for deltas are explored, and in section 6, conclusions are drawn.

2. Physics of Tidal Rivers

2.1. Phenomena Observed in Tidal Rivers

Perhaps, one of the most widely known phenomena observed in tidal rivers is the tidal bore [e.g., *Favre*, 1935; *Lemoine*, 1948; *Serre*, 1953; *Benjamin and Lighthill*, 1954; *Peregrine*, 1966; *Lynch*, 1982; *Chanson*, 2009; *Bonneton et al.*, 2012]. Bores are readily observed as a near-vertical wall of water traveling upriver during flood tide over tens of kilometers, often upstream of shallow estuaries subject to a relatively large tidal range. Under those circumstances, the difference in wave propagation celerity between the crest and the trough of a tidal wave may cause the occurrence of a solitary wave prior to complete dissipation of the tidal wave energy. For an observer standing on the bank of a river, the velocity is downstream prior to arrival of the bore (u_1) and upstream after passage of the bore (u_2), when the water level is lower. Hence, there is a nearly instant switch from flood to ebb in which the water depth increases from h_1 to h_2, where the subscripts 1 and 2 refer to the situation before and after arrival of the bore (respectively).

In hydraulics, the local phenomenon is referred to as a hydraulic jump. The speed at which the bore moves upstream, relative to the mean river flow, corresponds to the speed of a hydraulic jump [*Henderson*, 1966]:

$$c_g = \sqrt{\frac{gh_2(h_1 + h_2)}{2h_1}} \tag{1}$$

which was confirmed from field observations [*Wolanski et al.*, 2004; *Simpson et al.*, 2004]. The Froude number ($Fr = u/\sqrt{gh}$) can be used to evaluate if water in a tidal river flows ($Fr < 1$, subcritical flow) or shoots

Figure 2. Tidal bore on the Amazon River, locally termed Pororoca, composed of a primary wave that acts as a hydraulic jump, and secondary waves named whelps, which reduce amplitude with distance from the primary wave. The wave is propagating to the right. Photo courtesy: Carrie Vonderhaar/Ocean Futures Society/National Geographic Creative.

($Fr > 1$, supercritical flow). On either side of a tidal bore, conditions are subcritical, whereas the bore itself is supercritical. The surge Froude number is thus larger than unity and quantifies the intensity of the bore as in

$$Fr = \frac{c_g + u_1}{\sqrt{gh_1}} \tag{2}$$

Tidal bores can be undular or breaking. Undular tidal bores occur most often and are characterized by a train of advancing free-surface undulations, called whelps (Figure 2). Breaking bores are rare, often restricted to spring tide conditions and localized in particularly shallow sections. Much of the tidal bore wave train structure and breaking processes have been captured in laboratory experiments, analytical models, and numerical simulations, revealing turbulence properties and implications for sediment transport, morphology, and ecology along the section where the tidal bore acts.

The prediction of tidal bore occurrence from channel properties, tidal characteristics, and discharge remains a challenge. Building on the previous scaling analyses [e.g., *Friedrichs and Aubrey*, 1994; *Lanzoni and Seminara*, 1998], *Bonneton et al.* [2015] propose that tidal bore occurrence can be evaluated based on two dimensionless parameters: $\mathcal{D}_i$, representing the importance of energy dissipation relative to local inertia of the flow and K, measuring the kinetic effect of channel convergence relative to the effect of temporal oscillation of the free surface:

$$\mathcal{D}_i = c_f \frac{u_0}{h_0 \omega_0} \tag{3}$$

$$K = \frac{u_0 h_0}{a_0 \omega_0 L_{b0}} \tag{4}$$

where u_0, h_0, and a_0 are characteristic values of tidal velocity, water depth, and tidal amplitude at the mouth (respectively), L_{b0} is convergence length of the tidal river, ω_0 is tidal angular frequency, and c_f is the flow resistance factor or friction coefficient. *Bonneton et al.* [2015] propose that tidal bores occur in channels where K is about unity and $\mathcal{D}_i$ is large. The condition $K = 1$ implies that tidal bores typically appear in strongly convergent channels. For $K = 1$, $\mathcal{D}_i$ can be written as [*Lanzoni and Seminara*, 1998]

$$\mathcal{D}_i = c_f \frac{a_0 L_{b0}}{h_0^2} \tag{5}$$

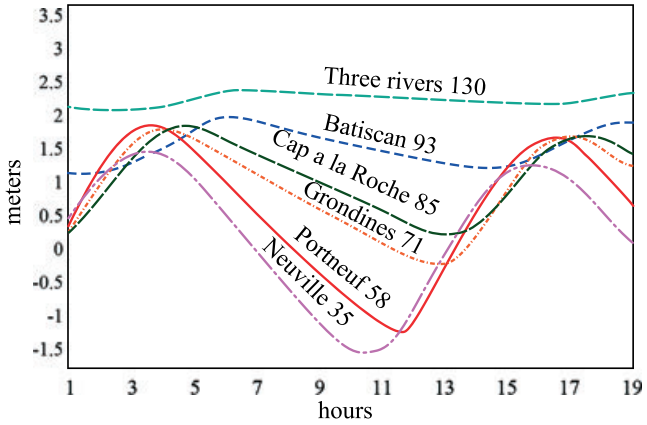

Figure 3. Simultaneous records of sea level on the Saint Lawrence River. Numbers after the gauge station names indicate the distance to the coast, in kilometer. Modified from *LeBlond* [1978], based on data in *Dohler* [1964].

This approach shows how tidal bore occurrence depends on friction, tidal amplitude, channel convergence, and depth but does not take into account the effect of the river discharge. Both the local tidal bore characteristics and processes of tidal propagation governing tidal bore occurrence depend, however, on local geometrical characteristics and, more importantly, on the river discharge [*Bonneton et al.*, 2015].

A tidal bore is an asymptotic case representing an extreme deformation of an astronomical tidal wave in a river that does not occur in most tidal rivers. Instead, tidal energy is dissipated as a consequence of bottom friction and the braking effect of the river discharge prior to reaching the stage of a tidal bore. Figure 3 shows simultaneous records of surface level along the Saint Lawrence River [*LeBlond*, 1978], representing a common development of a tidal wave: the amplitude systematically decreases in the upstream direction, and the phase lags are much larger for the occurrence of low water than for high water, implying that the tidal wave celerity is faster at high water than at low water [e.g., *Dronkers*, 1964; *Cai et al.*, 2014a]. Also, the tidal wave can travel against a mean water level slope. In other words, the absolute surface level during high water increases in the upstream direction. The tidal wave becomes progressively more asymmetrical, but clearly, the wave energy has dissipated prior to the coincidence of high water and low water in the upper reach of the river. The increase in asymmetry of tidal waves in a river is a general phenomenon that can be viewed as the development of superharmonics, i.e., waves with a frequency that is an integer multiple of the carrier wave, which can be diurnal (once daily) or semidiurnal (twice daily). Thus, a distorted wave as in Figure 3 can be decomposed into a set of simple harmonics.

Especially in tidal rivers where the river discharge is the same order of magnitude as the tidal discharge amplitude, the effect of the tide does not disappear when signals are averaged over a tidal cycle. Figure 4 shows a sequence of simultaneous water level recordings at the Yangtze tidal river, and a time series of discharge at an upstream location [*Guo et al.*, 2015]. The tide-averaged water levels, indicated in red, show an apparent coherence both with the upstream river level variation and with the tidal amplitude at sea. Mean water levels are higher at spring tide and lower at neap tide, which is best seen at a station in Nanjing. This fortnightly variation can be represented as a subharmonic of the principal D_2 tidal wave, caused by quadratic nonlinear interactions of the M_2 and S_2 tidal constituents that are responsible for the neap-spring variations in tidal range. It is also visible in Datong discharge series. The tidal component of fortnightly oscillations may be difficult to discern visually in the data, because river discharge waves generated by rainfall or at hydropower stations may bear a similar frequency. As we discuss below, quadratic and cubic interactions between tidal constituents give rise to a large number of subharmonic and harmonic oscillations at frequencies that are sums and differences of the basic tidal constituents. These oscillations are referred to as overtides.

2.2. Tidal Long-Wave Propagation

Except for local phenomena such as the secondary waves superimposed on a tidal bore (termed whelps, see Figure 2), the key tidal phenomena observed in tidal rivers can be described in terms of long-wave propagation. In the long-wave approach, the horizontal length scales considered are 10^3 to 10^4 times as large as the water depth, so a hydrostatic pressure distribution can be assumed. The behavior of long waves with friction became an urgent topic after the great storm surge of February 1953 that devastated much of the

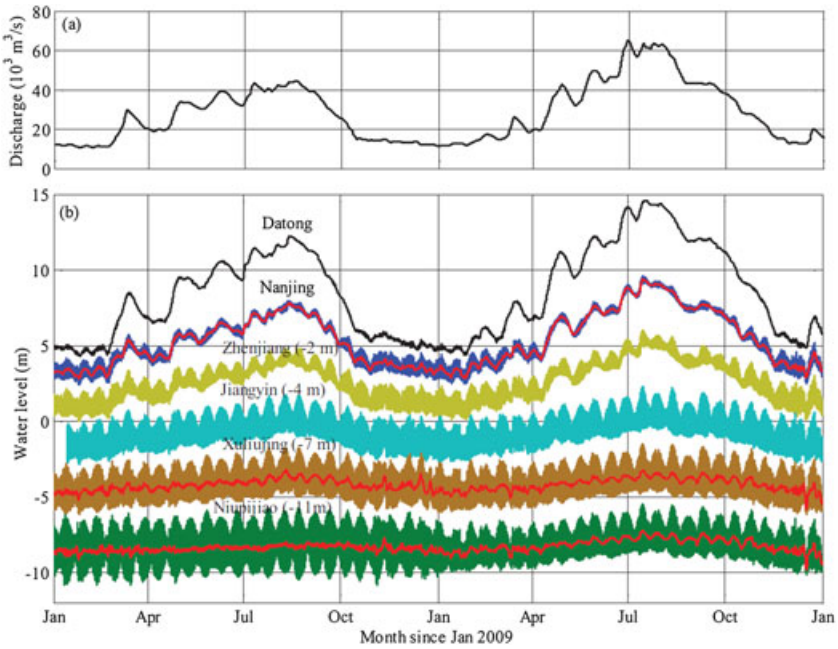

Figure 4. (a) Discharge of the Yangtze River for 2009 and 2010 at the head of the tide at Datong. (b) Simultaneous water levels at Datong, Nanjing, Zhenjiang (decreased by 2 m), Jiangyin (decreased by 4 m), Xuliujing, (decreased by 7 m), and Niupijiao (decreased by 11 m). These stations are, respectively, 600, 380, 280, 195, 110, and −50 km landward from the coast. The red lines indicate the daily (24 h) averaged mean water levels (MWL). Adopted from *Guo et al.* [2015].

coast of the southern North Sea. Research efforts begun in the Netherlands (as summarized in *Dronkers* [1964]), England [e.g., *Hunt*, 1964], and the U.S. [e.g., *Perroud*, 1958; *Dorrestein*, 1961]. In the absence of friction, there is also a formal analogy between propagation of a surface long-wave and a pressure wave, like sound [*Lighthill*, 2001]. However, this analogy breaks down for strong convergence in propagation area (the channel cross-sectional area for a water wave). A sound wave propagates smoothly through a convergent or divergent channel, up to a point. The divergent horn of early phonographs is an example of this kind of propagation, made famous by the dog listening to an RCA Victrola phonograph in an early advertisement. Beyond the point of "critical convergence" (defined below), an inviscid wave can only break up or dissipate, but not propagate. Interestingly, the presence of friction allows long waves like tides to propagate even in very strongly convergent or divergent channels [*Jay*, 1991]. The explanation is as follows. An inviscid one-dimensional wave equation, being second order and linear, admits two solutions: the incident and reflected waves as in basic fluid mechanics. Each of these has elevation and transport exactly in phase; i.e., they are "progressive waves." In the case of total reflection, the incident and reflected waves will combine into a "standing wave" with transport and elevation out of phase by 90°. This standing wave is an abstraction, and it cannot exist in a frictional environment, except at the point of reflection. In fact, the reflected wave is important in the strongly frictional tidal river environment only in the vicinity of very sharp constrictions. Adding the effects of friction to the second-order wave equation provides, however, an extra "degree of freedom" to the wave solutions. Even though there are still only two solutions, the incident wave (and the reflected one also, though it is not physically important) can have any phase difference between 0 and 90°. Thus, the incident wave can act as if it were being partially reflected without actually losing energy to reflection, and its propagation through a constriction is continuous.

Long-wave behavior can be captured in the one-dimensional conservation equations of mass and momentum integrated over the cross section [*Green*, 1838], generally referred to as the Saint Venant equations [*Saint-Venant*, 1871], which are readily numerically solved [*Dronkers*, 1964]. Numerical solutions are, however, of little help to understanding the qualitative behavior of river tides [*LeBlond*, 1978]. For this reason, many efforts have been undertaken to idealize channel geometry and derive analytical solutions ever since *Green* [1838], who also developed Green's functions. *Green* [1838] showed that an inviscid wave in a channel of slowly varying h and b defined in Figure 5, ζ varies as $b^{-1/2}\ h^{-1/4}$, while Q varies as $b^{1/2}\ h^{1/4}$ (Green's law). The different behavior of the tide with variations in depth and width results from the dependence of celerity

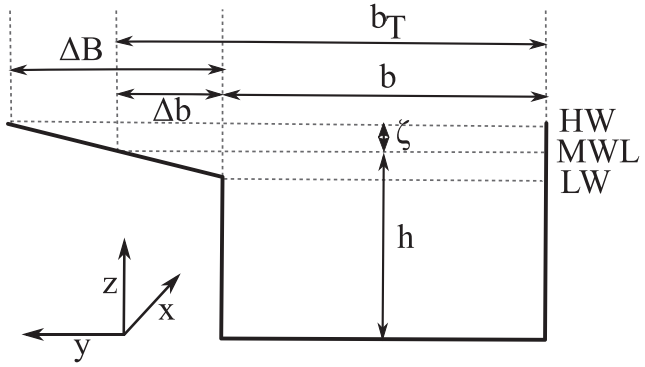

Figure 5. Geometrical definitions indicating mean water level (MWL), high water (HW), low water (LW), $\Delta B(x,t)$ as the time-varying tidal flat width, $\Delta b(x,t)$ as the mean tidal flat width, b as the momentum conveying width, b_T as the total width, h as mean depth, and ζ as tidal elevation above mean depth. Adopted from *Jay* [1991].

c on $h^{1/2}$. Among theoretical analyses that followed after *Green* [1838], the approach of *Jay* [1991] has yielded a synoptic wave equation that captures tidal long-wave propagation under the influence of a constant river flow velocity and the effect of tidal flats. Prior to discussing several key insights from alternative analytical models, we introduce tidal long-wave propagation using the latter model equation.

Jay [1991] followed *Aubrey and Speer* [1985] by assuming momentum is lost on the tidal flats during rising tide, caused by strong friction. Second, he assumed the energy loss on the tidal flats to be small compared to that in the main channel. By schematizing the river cross section according to the definitions in Figure 5 and assuming h and b vary exponentially in the along-channel direction, the Saint Venant equations can be combined in a single second-order wave equation for the discharge Q, which reads

$$\frac{\partial^2 Q}{\partial x^2} - \frac{1}{b_T}\frac{db_T}{dx}\frac{\partial Q}{\partial x} - \frac{3b_T - b}{g\bar{A}}U_R\frac{\partial^2 Q}{\partial x \partial t} + \frac{2b_T}{g\bar{A}^2}U_R\frac{d\bar{A}}{dx}\frac{\partial Q}{\partial t} - \frac{b_T}{g\bar{A}}\frac{\partial^2 Q}{\partial t^2} - \frac{b_T}{\rho g h}\frac{\partial \tau_b}{\partial t} = 0 \tag{6}$$

Herein, $\bar{A} = hb$, U_R is the river flow velocity, ρ is water density, b_T is the width during high water, and τ_b is the bed shear stress. The first term on the left-hand side of the equation (6) arises from the surface level gradient, the second from the surface level gradient and the tidal flat topography, the following two are convective accelerations, the next is the temporal acceleration term, and the last is bed shear stress, which can be represented by two first-order terms [*Jay*, 1991]. Equation (6) is a second-order linear differential equation with two solutions; these represent the incident wave from the ocean, and a reflected wave, which is often small in shallow channels. It shows the convective acceleration terms are linearly dependent on the river flow velocity U_R, which increases in the upstream direction. Both the river discharge and the tidal flats have a retarding effect on tidal wave propagation, which is fastest during high water, when depths are largest.

2.3. Insights From Analytical Solutions

LeBlond [1978] was among the first to recognize that the effect of inertia is limited for a large portion of the tidal cycle, so that the terms representing the surface level gradient and friction nearly balance, as do acceleration and convergence. Neglecting inertia in the equation of motion results in a nonlinear diffusion equation, which led to the notion that to a large degree, tidal behavior can be regarded as a diffusion process, which particularly holds well near full ebb. *LeBlond* [1978] solved the resulting diffusion equation he found, to explain the difference between the low-water propagation speed apparent in Figure 3 and predictions according to inviscid wave theory.

Friedrichs and Madsen [1992] elaborated on the approach of *LeBlond* [1978] to find analytical expressions for subharmonics, also termed zeroth harmonics, and superharmonics, also termed higher-order harmonics, as well as a solution for the main incoming tidal wave, including the effect of tidal flats. *Friedrichs and Madsen* [1992] introduced a parameter γ that quantifies the importance of depth variation relative to width variation caused by tidal flats: $\gamma = \frac{5}{3}A_\zeta/h - (b_T - b)/b$, where A_ζ is the tidal elevation amplitude. When $\gamma > 0$, time variations in channel depth are dominant. Attenuation is then stronger near the crest of the waveform than near the trough. The crest attenuates landward faster and decays slower than the trough. This results in a short,

rapid flood and a long, slow ebb, a setup of the mean elevation and (neglecting other factors) a tendency for landward sediment transport. If the effect of width variation is more important than depth variation, $\gamma < 0$, and the wave is ebb dominant. The attenuation is then larger near the trough of the waveform; the trough diffuses faster and decays slower, and the tide has a short, rapid fall, and the mean elevation is set down.

Based on a scaled version of equation (6) and adopting the approach of *Dronkers* [1964] to represent the friction term, *Jay* [1991] retained the inertia terms to revisit Green's Law [*Green*, 1838]. Standard and critical solutions were introduced that together span the complete range of physically realistic parameter settings. The standard solution holds when acceleration and topographic convergence are dominant over friction in determining the tidal wave length, which can hold for either weak or strong channel convergence. For the standard solution, the discharge amplitude varies as $b^{1/4}b_T^{1/4}h^{1/4}$ and the elevation amplitude as $b^{-1/4}b_T^{-1/4}h^{-1/4}$, which reduces to Green's Law when $b = b_T$. It holds approximately for weakly frictional channels, but tidal flats, strong friction, or strong convergence modify this result, sometimes strongly [e.g., *Lanzoni and Seminara*, 1998].

The seaward part of many estuaries and the lower part of the subsequent tidal river are often close to a condition of critical convergence, in which the acceleration and convergence terms in the wave equation balance one another, so friction determines wave celerity and wave length, and the phase difference between Q and ζ is about 45°. With this sort of "topographic funneling," a nearly constant wave amplitude can be maintained over considerable channel length, even in the presence of river flow. In this solution, the discharge and surface elevation amplitudes depend on $h^{1/2}$ and $h^{-1/2}$, respectively. *Jay* [1991] argues that the balance of friction and acceleration determines the phase difference, and that an incident long-wave can have any phase difference between ζ and Q from 0 to 90°, even in the absence of a reflected wave. Because the reflected wave is almost always quite weak in a shallow, strongly convergent channel, the common interpretation of tidal propagation as a mix of "progressive" and "standing waves" is usually misguided. A standing wave can only exist in a frictional channel at the point of reflection.

The above theory describes the behavior of a single harmonic as a starting point, representing the main tidal species in an estuary. A tidal species is a group of tidal constituents with similar frequencies. The astronomical tidal species have frequencies near 0, 1, 2, and 3 cycles d^{-1}, which we refer to as the D_0, D_1, D_2, and D_3 species. At the river mouth, multiple species can be present, including superharmonics generated in the adjacent shallow coastal sea. Nonlinear hydrodynamic processes in estuaries and tidal rivers may then add species from 4 to 14 cycles d^{-1} (D_4 to $D_{1/14}$) and perhaps beyond [*Rossiter and Lennon*, 1968; *Uncles et al.*, 1991], whose behavior is not described by the above theory, because they are forced waves. While there are multiple nonlinearities in the tidal equations, the nonlinear character of the friction term in the equation of motion is one of the key reasons for interaction between tidal species and the river discharge. In line with the work of *Doodson* [1956, 1957] and *Godin* [1991a, 1991b], *Godin* [1999] showed that the product $u|u|$ in the equation of motion may simply be approximated as $u_m^2(Au' + Bu'^3)$, where u_m is the maximum velocity used to nondimensionalize u, resulting in u' ($u' = u/u_m$); A and B are known constants. Using this approximation and retaining the simple balance between surface level gradient and friction, *Godin* [1999] made a systematic inventory of the sources of self and mutual damping of the incoming tidal waves and the river discharge. *Godin* [1999] continued his analysis to specifically focus on the upstream portion of the tidal river, where the flow is unidirectional and rapidly becomes extinct. In this region, tidal components are damped uniformly by the river flow, tidal flats are less ubiquitous, and the channel width has typically converged to become nearly constant. By neglecting the effects of channel geometry, *Godin* [1999] showed how damping in the upstream reaches depends on river flow, the friction coefficient, and the angular frequency of the tidal wave; higher-frequency waves are damped more rapidly. In the upstream regime, defined as the region where the tide is nearing extinction and tidal velocity oscillations occur around the equilibrium maintained by the discharge, the equations of motion are approximately linear. This allows multiple tidal waves to propagate independently. Interactions among tidal waves and the river flow are, thus, strongest in the downstream stretches of the tidal river, whereas upstream of this interaction region individual tidal waves coexist and can be analyzed in isolation.

Elaborating on theoretical work by *Savenije* [1992, 1998, 2001], *Horrevoets et al.* [2004] derived an analytical expression that yielded further insight into tidal dynamics in the upstream reaches of tidal rivers. They revealed the consequences of the fact that the discharge Q_R is imposed at the upstream end of the tidal river, rather than the velocity U_R. During low water, the river discharge is forced through a relatively small cross section, which can be the main reason for the reduction of tidal amplitude by the river discharge in the region

landward of the upstream limit of flow reversal. Obviously, this yields an asymmetrical attenuation over the tidal cycle. *Cai et al.* [2012] revised on the work of *Horrevoets et al.* [2004] and arrived at a new, improved formulation, used to highlight the sensitivity of tidal damping to river discharge, influenced by reservoir building, and depth, affected by dredging.

2.4. Tidal River Definitions

A tidal river occupies the semantically ambiguous junction between river and estuary, and its boundaries lack accepted definitions [*Pethick*, 1984; *Schwartz*, 2005]. Coastal oceanographers often define the landward boundary of an estuary (potentially the seaward boundary for the tidal river) in terms of salinity intrusion, but the source usually cited for this definition [*Cameron and Pritchard*, 1963] does not actually establish such a usage. *Cameron and Pritchard* [1963] define an estuary as "a semienclosed coastal body of water, which has a free connection with the open sea and within which sea water is measurably diluted with fresh water from land drainage." This definition is essentially geomorphic (a "semienclosed basin") and leaves open the extent of the system, whether brackish water occupies all of it, and the nature of the boundaries, which must be to some extent open to allow sea water and river flow to enter.

Definition of estuarine boundaries in terms of salinity intrusion is not the only approach. In fact, etymology argues for a tidal definition of estuary. The word "estuary" comes from the Latin *aesthus*, meaning tide [*Guilcher*, 1958; *Schwartz*, 2005]. This is essentially the definition adopted by *Fairbridge* [1980] who defined an estuary as "an inlet of the sea reaching into a river valley as far as the upper limit of tidal rise." In a similar vein, *Caspers* [1967] mentions that "the upper limit of the estuary is determined not by salinity but by tidal forces. In other words it is determined hydrodynamically rather than hydrochemically." In this definition the tidal river becomes a subdivision of the larger estuary, which is neither useful for our purposes nor entirely accurate, because it does not distinguish between the main tidal constituents and nonlinear tides at other frequencies.

The extent (often hundreds of kilometers) and distinct nature of the freshwater-tidal environment argue for a specific definition of tidal river. Accordingly, *Day et al.* [1989] divided the "estuarine system" into three components: a "tidal river zone," the "estuary proper," and a "nearshore turbid zone" including the tidal plume, using the extent of salinity intrusion to distinguish the tidal river. *Barendregt and Swarth* [2013] follow this usage with respect the distinction between the tidal river and estuary, whereas *McLusky and Elliott* [2007] note that the European lands are, for management purposes, free to choose the landward estuarine boundary anywhere between the limits of salinity and tidal intrusion.

While defining the estuary-tidal river boundary in terms of salinity may be functional for some systems with little variability in river flow, it is not useful for systems where the limit of salinity intrusion varies over many kilometers seasonally, and important habitats experience only seasonal salinity effects. Also, a different approach is suggested by the very distinctive inundation characteristics of the more landward reaches of a tidal river, where the annual cycle of river stage variation is much larger than the tidal range, and tidal range variability is controlled primarily by river flow.

Fortnightly oscillations increase almost up to the limit of the daily tide and may persist further landward, even when the D_1 and D_2 constituents of the tide are no longer observable. This suggests a definition of tidal river that is consistent with both the Latin *aesthus*, and with the *Cameron and Pritchard* [1963] definition. *Jay et al.* [2015] suggest, based on analyses in the Columbia, that the seaward boundary of the tidal river should be placed at the point where the lowest water levels occur on neap rather than spring tides. This occurs because, in these upriver reaches, the subtidal nonlinear oscillations are larger than the subtidal variations of daily tides. Herein, subtidal refers to oscillations with periods significantly larger than one day. This feature is easily seen in tidal records or in regression model results [cf. *Jay et al.*, 2011, 2016] (Figure 6).

We further propose that the tidal river extends landward to the point where both daily and subtidal oscillations have extinguished, unless a physical barrier (e.g., a dam or a rapid) provides an artificial limit to the tidal river before that point. For those who prefer a single term for the entire reach between salinity intrusion and the upstream tidal boundary, "tidal freshwater zone" seems appropriate. Our choice of boundary recognizes, however, that the tidal freshwater river encompasses zones with very different physics. In terms of tidal constituents, the reason that the lowest low waters occur on neap tides in more landward reaches can be explained as follows. Imagine a tidal river with two tidal constituents: M_2 and S_2. Nonlinear friction will generate the compound overtide MS_4, at the sum of the two frequencies and the fortnightly M_{sf} at their

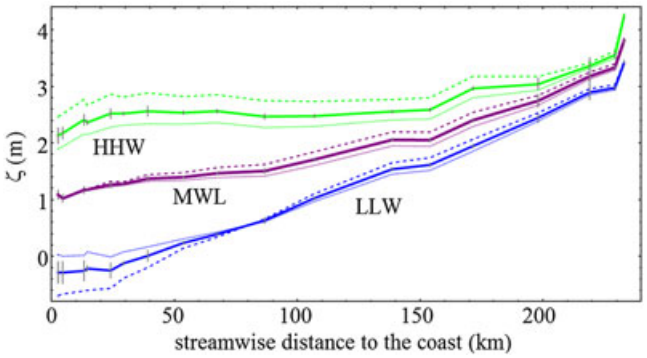

Figure 6. Lower low water (LLW, blue), mean water level (MWL, purple), and higher high water (HHW, green) as a function of river kilometer in the Columbia estuary and tidal river for typical mean (solid), neap (dotted), and spring (dashed) conditions and low river flow (3000 m^3 s^{-1}), from data summarized in regression models [*Jay et al.*, 2011, 2015, 2016]. Station locations and model standard 95% confidence limits are shown by the grey lines. Larger standard deviations and irregularities in the curves correspond to short records (near the mouth) or large power-peaking effects (upriver). Note that MWL and HHW are systematically higher on spring tides than on neap or mean tides. However, because river stage is much lower on neap tides, the lowest water level landward of Rkm-87 occurs on neap tides. Thus, the area landward of Rkm-87 up to the extinction of the tide at a dam at Rkm-234 is the tidal river.

frequency difference. The M_{sf} oscillation is mainly caused by the fact that during spring tide, a higher surface level slope is needed to realize the same discharge than during neap tide. It grows upriver and may outlast the main tidal constituents (here, M_2 and S_2, with amplitudes A_{M_2} and A_{S_2}, respectively), so that there is little daily tide but still a fortnightly oscillation far upriver. Spring and neap tides are represented by M_2 and S_2 being in phase or out of phase, with the spring tide amplitude equal to $A_{M_2}+A_{S_2}$ and a neap tide amplitude of $A_{M_2}-A_{S_2}$. The period of M_{sf} exactly corresponds to the duration of a spring-neap cycle. It lowers the daily-averaged levels during neap tide and raises it during spring tide. At some point along the channel, the amplitude of M_{sf}, $A_{M_{sf}}$, becomes equal to A_{S_2}. That is where the reversal of the lowest low waters from spring to neap occurs. Additional tidal constituents make the algebra messier but do not change the essential physics. This definition of tidal river has also been found useful in the Yangtze [*Guo et al.*, 2015] and the Saint Lawrence [*Matte et al.*, 2014], and it could be applied to the Amazon [*Gallo and Vinzon*, 2005]. The occurrence of the lowest water levels on neap tides is also a matter of considerable importance for tidal river navigation. Finally, this seaward boundary of the tidal river may also nearly coincide with the point at which the amplitude of the annual river stage cycle is about the same as the maximum tidal range during low-flow periods.

These tidal river boundary definitions should be reasonably universal, in that all tidal rivers have nonlinear tides, and the long wavelengths of these nonlinear tides mean that they can persist far landward, regardless of the convergence rate of the channel cross section. These definitions are also applicable to situations, like the Amazon, where there is no salinity intrusion at all (Table 1). The Congo River [*Savoye et al.*, 2009] is a possible (and unique) example with its 500 m deep estuary, but too little is known about its tides to draw conclusions.

Table 1. Estuary and Tidal River Properties for the Amazon [*Gallo and Vinzon*, 2005], Columbia [*Jay et al.*, 1990, 2016], Saint Lawrence [*Matte et al.*, 2014], and the Yangtze [*Pu et al.*, 2015; *Guo et al.*, 2015][a]

	L_{sal} (km)	L_t (km)	L_h (km)
Amazon	0	400–500	1000
Columbia	5–50	87	234
Saint Lawrence	500	600	730
Yangtze	50–100	380	600

[a]Estimates of salinity intrusion length L_{sal} and the distance between the seaward and landward tidal river boundaries and the coast (L_t and L_h, respectively). Landward of L_t, LLW during spring tide typically exceeds LLW during neap tide, whereas seaward of L_t, the opposite holds. At L_t, $A_{M_{sf}} \approx A_{S_2}$. L_l estimates the head of the tide, where the tidal motion has become extinct. The tidal freshwater zone is in between L_{sal} and L_h.

A more likely issue with the above definitions is that they could prove, like a salinity-based definition, to be seasonally variable in some systems. In that case, we suggest the usual seasonal maximum tidal intrusion during low-river flow periods be considered in setting the definitions. In the Columbia, it was found that the seaward boundary of the tidal river coincided with a hard rock channel constriction and (approximately) with a vegetation boundary. Multiple linear regression analyses of lower low water (LLW) against river flow and near-ocean tidal range show that the location of the boundary did not vary with flow [*Jay et al.*, 2015, 2016], and analyses of data collected in 1940–1943 show that it has moved very little, if at all, over a 70 year period, despite deepening of the channel from 9 to 13 m. The point at which the tide is extinguished does, however, show seasonal variability in the Columbia.

There is one other semantic issue relevant to tidal rivers. The usual definitions of mean lower low water (MLLW), mean higher high water (MHHW), and other tidal datum levels are difficult to determine in an environment where seasonal stage variations are larger than the usual tidal range. A precise definition would require averaging over both the timescales of flow variability and the 18.6 year lunar nodal period. The lunar nodal period is the time between either of two nodes corresponding to the locations where the Moon's path in space crosses the ecliptic, which is the Sun's path in space. The definitions of MLLW and MHHW are further complicated by the fact that tidal-fluvial environments often exhibit strong changes in bathymetry due to engineering processes that are causing tides to evolve [*Jay et al.*, 2011; *Vellinga et al.*, 2014]. It seems useful to define low water (LW) for dominantly D_2 environments or LLW for mixed D_1 and D_2 systems as a function of flow, ocean tidal range, and any other relevant parameters (e.g., coastal sea level or winds). Similar procedures can be used for high water (HW) or higher high water (HHW), and mean water level (MWL). This usage is generally consistent with the definitions provided by *International Hydrographic Organization* [1994], where LLW, MWL, and HHW are averages over an unspecified period, rather than fixed datum levels. Both the unsteady nature of tidal river boundaries and the difficulty of defining tidal datum levels explain inconsistent use of the term tidal river. Throughout this manuscript, the term tidal river is to be interpreted sensu lato, i.e., including the freshwater part of the estuary.

3. Methods of Time Series Analysis

3.1. Tidal Analysis Strategies for Nonstationary Environments

Analysis of river tides is complicated by the large number and wide range of frequencies (periods of about 1 h to 18.6 years) arising from astronomical tidal forcing (475 according to *Cartwright and Tayler* [1971]) and the many hundreds of additional frequencies that can arise from nonlinear hydrodynamics processes. Each of these frequencies represents a so-called tidal constituent (see also section 3.2), and the more important ones have been given a symbol composed of a letter representing the astronomical origin and a number representing the frequency. For example, S_1 is the principal solar diurnal tide, with a period of 24 h.

It is normal that a tidal record has too short a length of record, abbreviated LOR, to quantify all relevant low-frequency processes and has too long a sampling interval, Δt, to accurately determine the highest tidal frequencies. River tides are, moreover, highly nonstationary, and the sampling problem is complicated by the need to capture the relevant timescales of stochastic fluvial processes (typically decades) in addition to tidal variability. A "stationary" process in this context is one for which all subsections have similar statistical properties. As for most nonstationary systems in geophysics, there is no single tidal analysis approach that provides all the information needed to address the dynamics of tidal-fluvial regimes. It is common, therefore, to begin an analysis of river tides by application of analysis tools meant for stationary processes, followed by use of more specialized tools for nonstationary tides. We follow this trajectory in describing the analysis approaches used for analyzing river tides, in sections 3.3 to 3.5.

Stationary analysis tools (e.g., harmonic analysis) are, because of their underlying assumptions and mathematical apparatus, more commonly used for prediction, whereas nonstationary analyses approaches (e.g., wavelets) can, if properly used, provide deeper dynamical insights. Hybrid approaches can potentially do both but are still limited in their range of applicability. Figure 7 shows a conceptual view of tidal-fluvial water level approaches. A key decision is whether the record should be treated as stationary or nonstationary. While this decision depends to some extent on the purpose of the analysis, the degree of nonstationarity should be quantified; e.g., by use of harmonic analysis or wavelet tools designed for this purpose. Even if the record is determined to be strongly nonstationary, stationary analysis tools can provide important insights, though they may not provide useful predictions. One commonly used stationary tool is power spectral analysis. Power

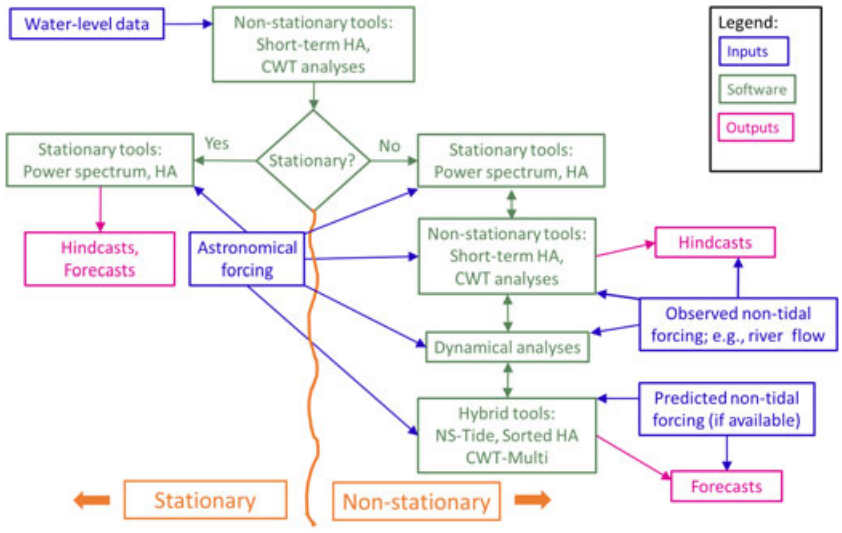

Figure 7. Conceptual view of tidal analysis procedures for stationary and nonstationary water level data. An initial application of short-term harmonic analysis (HA) or continuous wavelet transform (CWT) analysis is needed to determine whether a stationary or nonstationary analysis path is appropriate, and application of stationary tools is a usual starting point for analysis of nonstationary records. Thus, there is some duplication of the two paths in the early stages.

spectra and related tools are generic; their oceanographic application is described in standard references such as *Thomson and Emery* [2014]. Harmonic analysis is discussed in section 3.2. Figure 7 emphasizes that additional information and more complex procedures (discussed in sections 3.3 and 3.4) are needed to provide process understanding and water level predictions from nonstationary data. Such predictions are possible only to the degree that the nontidal process (e.g., the river flow) is not truly random. Thus, useful preliminary water level predictions can sometimes be prepared for tidal rivers several months or a year in advance, based on hydrologic forecasts and/or typical season flow curves.

In summary, tools designed for analyzing stationary data are often used for preliminary analyses of nonstationary data, but it is easier to analyze the interactions of tidal and nontidal processes with nonstationary analysis tools, rather than tools that presume that such interactions are absent or negligible. To quote [*Munk and Cartwright*, 1966] "It can be said that we are here attempting to improve the only geophysical prediction that works tolerably already; to this charge we plead guilty. But predicting and learning are in a sense orthogonal, and the most interesting effects are those that cause the most trouble with forecasting: the continuum, the nongravitational tides, and the nonlinear interactions."

3.2. Stationary Analysis Tools: Harmonic Analysis

Tides have traditionally been analyzed using "harmonic analysis" or HA. HA describes the tide in terms of a finite number of "tidal constituents"; i.e., sinusoidal waves with frequencies determined from astronomical and hydrodynamic theory, whose amplitudes and phases are determined by least squares regression analysis. Harmonic analysis originally assumed that the tides were the only process affecting water levels, and that tides were perfectly regular or stationary [*Darwin*, 1893; *Doodson*, 1921]; i.e., that they reflect the "the music of the spheres." This conceptual model implies that the water level power spectrum is made up only of discrete, extremely narrow tidal bands. A musical analog would be the unchanging sound of a group of tuning forks. Ironically, it is this highly reductive intellectual framework that makes HA attractive; its sinusoidal basis functions (the tidal constituents) are of infinite extent in time, allowing (for situations in which water levels are nearly stationary) hindcasts and forecasts to be made [*Flinchem and Jay*, 2000].

HA has frequency resolution and predictive ability unmatched by any other approach to tidal analysis, at least for water level data with sufficient LOR and a low noise level. It can also be applied to 2-D horizontal velocity (u, v) fields, though tidal currents are much more nonstationary than water levels at nearby gauges, making them hard to predict [*Godin*, 1983; *Jay*, 1991].

HA is implemented by minimization of the residual errors with respect to the harmonic constants, i.e., two per constituent, corresponding to the real and imaginary parts. This complex output can be resolved into an amplitude and phase. Because the system is always overdetermined (more equations than unknowns),

the minimization is usually implemented via a least squares (L2) norm regression [e.g., *Pawlowicz et al.*, 2002; *Foreman et al.*, 2009]. However, a "robust" solution that iteratively downweights outliers results in more accurate harmonic constants with tighter confidence limits, at least for noisy data [*Leffler and Jay*, 2009; *Codiga*, 2011]. In effect, the iterative robust solution reduces the norm from L2 toward a linear minimization (L1 norm). HA also uses a technique called "inference" to find a solution that includes in an approximate manner constituents that cannot be determined from the available LOR, given the ambient noise record. Inference is based on the assumption that amplitude and phase of undetermined tidal constituents bear a known relationship to constituents that can be determined.

Tidal records always exhibit at least a mild degree of chaos [*Frison et al.*, 1999; *Maas and Doelman*, 2002], and the above framework is insufficient for analysis of coastal processes in general and tidal rivers in particular, as suggested in Figure 7. Water level records are nonstationary because they reflect the influences of many processes, and in a tidal river, tides may account for only a small part of the variability. A first step in recognition of the nonstationary nature of tides was the incorporation of the effects of nontidal processes as background noise in the tidal record, interpreted as broadening of spectral peaks [*Munk and Cartwright*, 1966; *Cartwright*, 1968; *Godin*, 1972]. While *Munk and Cartwright* [1966] and *Cartwright* [1968] advocated a different form of tidal analysis, "the response method," based more closely than HA on the astronomical tidal potential, their method does not deal gracefully with the nonastronomical constituents that are so important in tidal rivers. For our purposes, the main impact of their work was the recognition of the impacts of nontidal processes on HA. If there is background noise caused by nontidal processes, then a statistical apparatus is needed to determine the validity of the amplitudes and phases derived from a harmonic analysis [cf. *Foreman*, 1977]. Also, noise limits the number of harmonic constituents that may be determined from any LOR [*Munk and Hasselmann*, 1964], and time variability of tidal properties (either real or due to instrumental effects) reduces the estimated amplitudes of some tidal constituents [*Zaron and Jay*, 2014]. Clearly, a proper statistical apparatus is vital, but even with this addition HA is not an optimum analysis tool for tidal rivers, neither conceptually nor practically.

Conceptually, water levels in tidal rivers reflect the interactions of fairly regular oceanic tidal forcing with stochastically varying river flow. Thus, the frequency content of the water level record is not static or stationary. It evolves over time, as does the frequency content of music. The human ear immediately recognizes the difference between a musical passage played forward and the same passage played backward and would give them different meanings [*Flinchem and Jay*, 2000]. Yet stationary techniques like spectral analysis and HA distinguish the forward and backward versions only via a change in phase (which disappears in the calculation of a power spectrum), and they cannot represent evolving frequency content at all. Applied to river tides, an HA averages over the tides and mean water level for all the different river flows during the period of the record analyzed, and water level predictions based on HA can be in error by many meters when applied to a tidal river.

An obvious practical response to the need to define evolving frequency technique is the use of "short-term HA," applied by dividing a water level time series into overlapping blocks, with a length set by the timescales of river flow variability; typically, the blocks or "windows" have a duration of a few days to a month. Short-term HA has several shortcomings [*Jay and Flinchem*, 1997, 1999]. The first is that it can define only a limited number of D_1 and D_2 constituents, thus providing only limited predictive ability and insight into river-tide physics. Also, it cannot define the properties of the subtidal fluctuations that play such a strong role in tidal river physics. Further, many rivers have significant variability on timescales of a few days. When HA windows are made this short, then analysis results are contaminated by nonlinear interaction terms (negligible for windows of 15 days or longer) that are strongest when the nontidal signal is varying strongly and one most needs accurate results. Finally, the power spectrum analysis of residual errors (the discrepancy between the data and a hindcast based on the analysis results) used to judge the significance of the constituent properties determined by an HA [cf. *Pawlowicz et al.*, 2002; *Codiga*, 2011] is of dubious validity for short-term HA.

The above problems of short-term HA stem in large part from the fact that HA lacks a well-defined frequency response [*Jay and Flinchem*, 1999]. That is, the response of an HA at a particular frequency is not a priori known. Rather, it depends on the length of the HA window, the frequency content of the data, and the other frequencies included in the analysis. This issue is most acute for the short HA windows that one would like to apply to the rapidly changing dynamics of a tidal river.

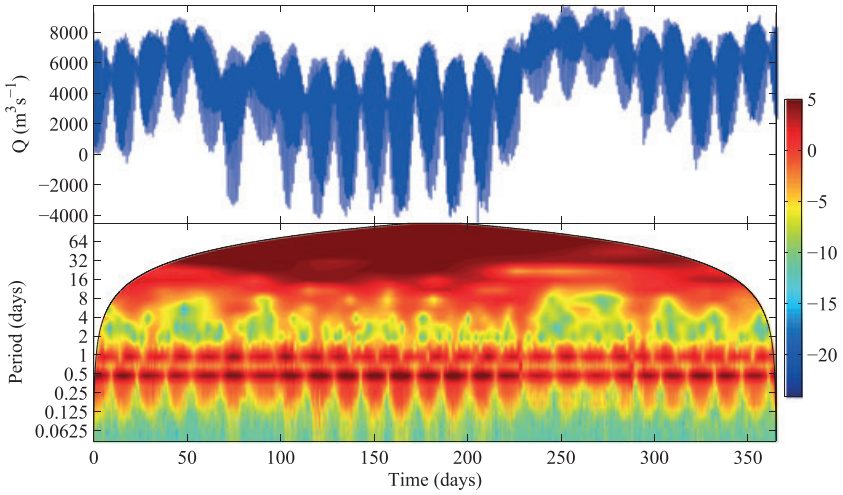

Figure 8. (top) Discharge series for the Mahakam River based on *Sassi et al.* [2011a] and the (bottom) corresponding continuous wavelet power spectrum. Colors indicate $\log_2(A^2)$, where A is the wavelet amplitude. Fortnightly cycles of D_1 and D_2 (spring-neap cycle) can be sharply observed. Variation of $D_{1/14}$ (period of 14 days) often interferes with variance directly introduced by the river discharge.

In summary, the use of stationary techniques like HA and spectral analysis in their usual forms is only a first step (though an important one) in analysis of river tides. Explanation of more sophisticated modified HA or hybrid HA-wavelet approaches (section 3.4) requires explanation of wavelet techniques, offered in section 3.3.

3.3. Wavelet Analysis of Nonstationary Tides

A wavelet transform extracts the frequency content of a signal as a function of time, such that the trade-off between time and frequency resolution is nearly optimal with respect to the Heisenberg uncertainty principle [*Rioul and Vetterli*, 1991]. The uncertainty principle is a property of the mathematical representation of waves. It says that there is an irreducible minimum product of the frequency uncertainty $\delta\omega$ and time uncertainty δt for any representation of a wave process:

$$\delta\omega\delta t \geq (4\pi)^{-1} \tag{7}$$

where $\delta\omega$ and δt are analogous to standard deviations but have been normalized by the squared wave energy. To understand the Heisenberg uncertainty principle, consider a pure sinusoidal wave. A single data point localizes the signal in time within the sampling interval δt, but the frequency is completely indeterminate. A long time series (thousands of cycles) allows definition of the frequency with considerable accuracy, but the time localization is low. A practical analysis scheme for nonstationary data must balance these factors. Wavelet transforms come in two types: discrete and continuous [*Vetterli and Herley*, 1992]. A discrete wavelet transform provides optimal data compression, but the wavelets do not resemble physical waves. A continuous wavelet transform or CWT makes use of wavelets that may resemble real waves but is redundant. The CWT consists of more numbers than the original data, even though no new information has been created. Both types of wavelet transform provide a complete basis for a real signal, but the CWT basis functions have nonzero correlations, i.e., are not orthogonal, because of their redundancy).

A CWT can also be described by analogy to a Fourier transform; a regular grid of frequencies is used in both cases, but the sinusoidal basis functions of a Fourier transform localize the timing only to the time period of the series analyzed. Figure 8 gives an example for a 1 year time series of discharge in the Mahakam River, described in *Sassi et al.* [2011a]. Wavelets are finite in time duration and are "convolved with" (moved through) the signal, so that a CWT provides information regarding evolving frequency content. However, the finite (short) length of the wavelets mean frequency resolution is much lower than with a Fourier transform, and outputs are usually provided less often for longer windows than short ones, consistent with the Heisenberg principle. Implementation of a wavelet transform requires definition of a type of wavelet to use. Wavelets should be "wave-like," and they must have finite length and energy, and zero mean. Also, if we want to estimate both amplitude and phase, a wavelet must be complex, having even (symmetric about the origin) and odd (antisymmetric) parts. A wavelet transform is based on a "mother" wavelet that is then altered in scale (i.e.,

inverse frequency) and temporal location for application to (i.e., convolution with) a time series. The wavelet transform apparatus can be summarized as follows. Wavelets of varying scale (s) and displacement from the origin (τ) are defined in terms of a mother wavelet Ψ [*Kukulka and Jay*, 2003a]:

$$\Psi_{\tau,s}(0) = N(s)\Psi\left(\frac{t-\tau}{s}\right) \tag{8}$$

$$\Psi(t) = W(t)e^{2\pi it} \tag{9}$$

where t is time, $W(t)$ is a window function that determines the length of the wavelet (in cycles), $N(s)$ is normalization, and there is an implicit scale $s = 1$ associated with the mother wavelet in equation (9). Both Gaussian [e.g., *Guo et al.*, 2015] and modified Bessel function [*Jay and Flinchem*, 1997; *Flinchem and Jay*, 2000] windows have been used for tidal analysis. The two types are known as Morlet [*Torrence and Compo*, 1998] and Kaiser-filter [*Kaiser*, 1974] wavelets, respectively; analysis results are similar. For most uses of wavelets, the normalization conserves the energy of the wave (proportional to scale as well as amplitude). For tidal analysis, it is customary to conserve amplitude; the correct normalization varies with W. The wavelet transform of a time series $z(t)$ is obtained by convolution of $z(t)$ with the wavelet filter bank:

$$Y_{\tau,s} = \int \Psi^*_{\tau,s} z(t)\mathrm{d}t \tag{10}$$

where the asterisk indicates a complex conjugate, and $Y_{\tau,s}$ is the forward transform into (τ, s) space. The frequency (inverse scale) of the mother wavelet is varied geometrically from the Nyquist frequency down to the longest wavelet that can be accommodated by the available LOR. As a rule of thumb, the window function should be about 6 wave cycles long for each scale, to resolve frequencies that differ by a factor of 2. Longer wavelet windows have better frequency resolution but poorer time resolution; there is no escape from the Heisenberg principle. Just as with a Fourier transform, there is an inverse wavelet transform, and both must be implemented in a discrete (in time), digital form, with the time resolution determined by the input data. While gappy data can be easily accommodated, irregular sampling intervals (e.g., available historic high-low tide data) would greatly slow a CWT analysis.

Most applications of wavelets are agnostic with respect to frequencies that might be present. For tidal analysis, however, the spacing of frequencies is often adjusted to accommodate known tidal frequencies [*Flinchem and Jay*, 2000]. This approach requires that the convolution be applied in the time domain. Alternatively, a dense, regular set of wavelet scales can be employed, with the energy for a given tidal species synthesized from adjacent wavelet outputs [*Guo et al.*, 2015]. This approach is faster and makes use of the Fourier transform of the data, but it does not work well with gappy data. Whichever approach is used, wavelets that resolve variations of tidal processes on timescales from a few days to a week (depending on frequency) cannot distinguish tidal constituents within a tidal species; the time variation of the tidal species as a whole is defined.

As will be discussed in section 3.4, longer wavelets can be used to distinguish tidal constituents within tidal species. However, in very nonstationary systems, tidal-fluvial interactions are so strong that it is appropriate to resolve only tidal species [*Jay and Kukulka*, 2003]. Also, the tidal constituent apparatus is a nonunique representation of the astronomical tidal potential, Γ [*Munk and Cartwright*, 1966]. As such, it has less physical meaning than the tidal species. Knowledge of both astronomical forcing (as Γ) and stochastic factors (e.g., river flow) is needed for useful dynamical analyses based on CWT analysis (cf. Figure 7). Time series of Γ are often used as a reference for the data being analyzed [e.g., *Moftakhari et al.*, 2013], because wavelets do not resolve tidal constituents. Thus, neap-spring (and other subtidal tidal) variations (caused by the various constituents within a tidal species) appear in the D_1, D_2 and higher-frequency outputs, complicating the analysis of the effects of nontidal forcing. Much of this variability is removed by use of Γ as a reference time series, because the neap-spring variability in Γ is similar to the time series of interest. Alternatively, a nearby coastal station can be employed as the reference for river tide analyses [*Simon*, 1991; *Jay and Flinchem*, 1997; *Kukulka and Jay*, 2003a]. This is useful, because use of a coastal reference removes both neap-spring effects and continental shelf perturbations of the tides. In practice, the CWT analysis is carried out on the observed data and the reference station data (sampled in the same manner as the observed data), then an "admittance" (A) is formed as the complex ratio of the station CWT output to the reference output for each scale and time.

A can be resolved into an amplitude ratio and a phase difference; the phase difference is analogous to the use of Greenwich phases in conventional HA programs. It is perhaps surprising that the astronomical tidal potential is not used more in tidal analyses (as suggested by *Munk and Cartwright* [1966]), a subject to which we return below.

To summarize, the great strength of CWT tidal analysis is that it can stably resolve rapid variations in tidal processes, facilitating dynamical analysis in a way that no other method can. Thus, CWT methods have a central role in analysis of nonstationary tides (Figure 7). Their use also encourages the point of view that the nonstationarity of tidal processes is an opportunity to obtain process understanding, not a disadvantage to be ignored or averaged away. Further, data errors like spikes affect only CWT outputs in the (time) vicinity of the errors, rather than the entire analysis, as would be the case for an HA or spectral analysis. Finally, CWT methods are very useful for analysis of tidally influenced or tidally varying processes (e.g., the productivity of particle attached bacteria [*Flinchem and Jay*, 2000]) that do have the regularity of water level data. CWT tidal analysis also has disadvantages. It is unable to distinguish constituents within tidal species, does not lend itself as readily to prediction as HA, and (like HA) lacks a good scheme for determining the significance of its amplitude and phase estimates. The usual approach for determining significance [*Torrence and Compo*, 1998] provides only global estimates based on average spectral properties of the time series, not local estimates specific to each output. Also, it assumes that the residual spectrum is either made up of normally distributed "white" noise or "red" noise (increasing toward low frequencies). Unfortunately, the tidal residual spectrum is neither white nor red; it has local energy increases (known as "cusps") in the vicinity of each of the tidal species.

3.4. Hybrid Analysis Techniques

A variety of approaches have been developed to improve the time resolution of HA or, conversely, to improve the frequency resolution of wavelet analysis techniques. All can be thought of as being ways to cheat on the limitations imposed by the Heisenberg uncertainty principle, usually by assuming that the tidal frequencies are known and do not need to be treated as uncertain, an assumption that is usually justified in the tidal river context. Even though the mean flow in a tidal river can be a substantial fraction of the wave celerity, tidal waves in rivers have a very small aspect ratio (wavelength to depth ratio) and retain a bed reference frame. This is not true for internal tides, which are sometimes Doppler shifted by an ambient current [*Mooers*, 1975] that moves their frame of reference, the interface, or stratified layers along which they propagate. Thus, the methods discussed in this section may not be applicable to internal tides, which is unfortunate, because they are often strongly nonstationary. Three methods will be discussed here. The first two are adaptations of HA to accommodate nonstationarity, while the third is a form of CWT analysis with improved frequency resolution.

The first method is NS_Tide [*Matte et al.*, 2013, 2014], which modifies T_Tide [*Pawlowicz et al.*, 2002] by using a robust regression and building nonstationary forcing into the solution basis functions. Rather than assuming that a tidal constituent *i* can be modeled as $\zeta_i = a_i \cos(\omega_i t) + b_i \sin(\omega_i t)$, with a_i and b_i constant for the period of record, the model used by NS_Tide for constituents at tidal river stations in the Columbia and Saint Lawrence Rivers is

$$\zeta_i = f_{a,i}\left(Q_R, T_R\right)\cos(\omega_i t) + f_{b,i}\left(Q_R, T_R\right)\sin(\omega_i t) \tag{11}$$

where Q_R is river flow, T_R is reference station tidal range, and $f_{a,i}$ and $f_{b,i}$ are polynomials (with unknown coefficients) taken from the analysis of *Kukulka and Jay* [2003a, 2003b]. Just as with a_i and b_i in a normal HA, the coefficients in these polynomials are determined by linear regression (here a robust regression). The net result is that there are six coefficients to determine per constituent, though unpublished work has also included atmospheric factors, leading to 8–10 coefficients per constituent.

A typical result is shown in Figure 9, which emphasizes that NS_Tide can represent river tides much better than conventional HA. To cover the range of tidal-fluvial interactions, however, several years of record are required.

Perhaps, the most important innovation in NS_Tide is the development of a new constituent selection criterion. This criterion uses the energy level in the low-frequency peak at the red end of the water level spectrum to determine whether two closely spaced (in frequency) peaks can be resolved, based on discussion by *Munk et al.* [1965]. In many cases in a tidal river, variability of river flow on timescales of 2, 3, 6, and 12 months means that the spectral energy of the major tidal constituents is smeared out over that of adjacent smaller peaks, making analysis results for the smaller peaks meaningless. Thus, even though a record exceeding 7 years was available for the station in the Columbia River shown in Figure 9, only seven constituents each

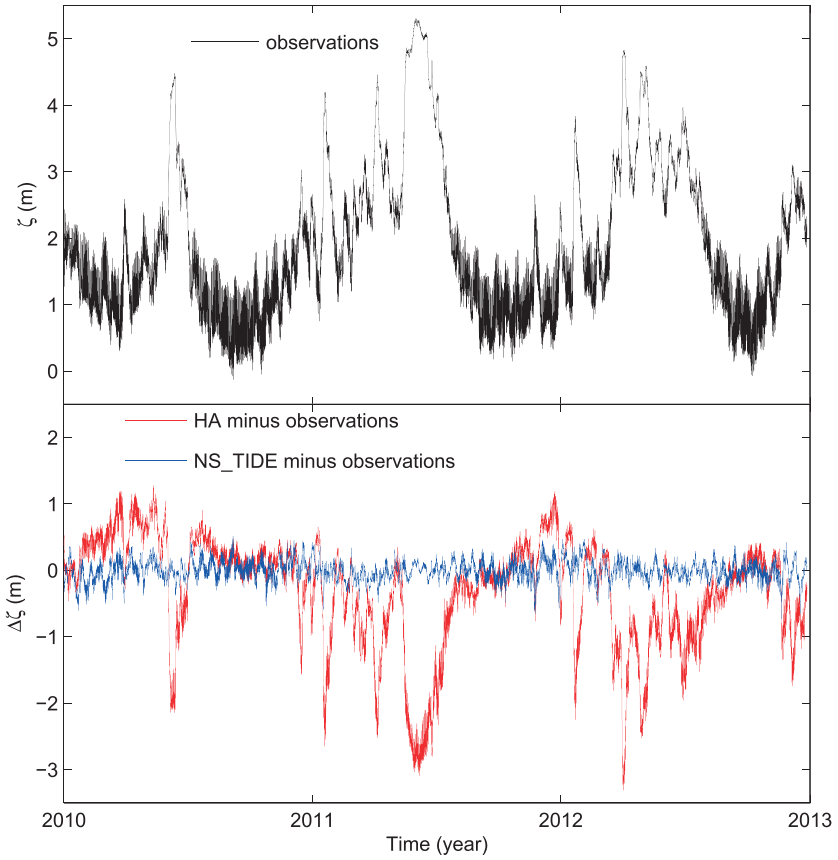

Figure 9. (top) Water level observations and the (bottom) difference with predictions for standard HA and NS_Tide at Vancouver, WA, from January 2010 to December 2012, a period with several high-flow event occurred (image courtesy of P. Matte). While this is something of a worst case scenario for HA, the result has general validity; NS_Tide more accurately hindcasts water levels in a tidal river than stationary HA; HA hindcasts can be inaccurate by 2–3 m and greatly overestimate tidal amplitudes during high-flow periods.

in the D_1 and D_2 species were selected, instead of the 30+ for each species normally used with a multiyear record. This application of NS_Tide demonstrates that accurately determining the time variation of a small number of the largest constituents results in better hindcasts than determining the time-average behavior of a large number of constituents. NS_Tide can also be used for prediction, if the annual river flow cycle is known, or based on hydrologic forecasts. It has, however, some disadvantages. For example, the exponents in f_a and f_b may need to be tuned iteratively, and the generality of the polynomials suggested by *Kukulka and Jay* [2003a, 2003b] remains unknown. Also, if too many or too few constituents are used, or if LOR is too small, then unrealistic results may be obtained. Thus, NS_Tide is not like a "point and shoot" camera. Care is required in its use.

Guo et al. [2015] use another HA approach to analysis of river tides in the Yangtze, referred to as nonstationary HA or NSHA. The water level record was separated into eight bins according to river flow, and the data in each bin were separately analyzed with robust T_Tide. This approach is facilitated by the fact that the flow in the Yangtze River varies annually only by a factor of 4 and usually varies slowly relative to the tidal month, so this binning of data did not lead to excessive fragmentation of the record. This approach provided a clear resolution of the dependence of tidal properties on river flow, even though there were too few high-flow days in the 8 year record to analyze tidal behavior during the highest flows. It does not, however, provide any insight into hysteresis effects (differences in tidal behavior during periods of rising and falling flow [*Sassi and Hoitink*, 2013]), and the formal statistical properties of the analysis have not been determined. Despite these possible issues, this technique is relatively robust and should be useful in systems that, like the Yangtze, do not exhibit rapid or excessive flow variability.

None of the analysis methods described above allows analysis of the variations of multiple tidal constituents within each tidal species on subtidal tidal timescales. Yet the importance of triad interactions (e.g., O_1-K_1-M_2 *Hoitink et al.* [2003]), the complexity of D_1 dynamics in rivers with mixed D_1-D_2 tides [*Godin*, 1999], and the evident temporal-spatial differences in behavior of major constituents like M_2 and S_2 [e.g., *Jay et al.*, 1990, 2015] argue that a method that can resolve such variations is needed.

We suggest that progress can be made in the area of nonstationary constituent resolution by combining the linearity of wavelet filters and analyses of each tidal frequency on multiple timescales with the traditional tidal analysis idea of inference, i.e., use of the known or estimated ratio of a minor constituent to a larger, nearby constituent to separate the two. Rather than the usual arbitrary specification of ratios of tidal constituents for inference, CWT filters of length 6 months to 1 year could be used to define time-varying constituent ratios objectively on a slow timescale. These ratios could then be used with CWT filters of length 2 weeks to 1 month (the fast scale) that separate the major constituents like Q_1-O_1-K_1 and N_2-M_2-S_2 that are not too closely spaced [*Jay*, 1997]. This is possible because wavelet filter linearity allows "cross talk" between frequencies in any set of filters to be removed, if the filter lengths are appropriate and the frequencies known. Unpublished work shows that once the major frequencies are separated on the fast scale, inference of frequency ratios from the slow scale can be used to resolve closely spaced constituents (e.g., the pairs K_1 and P_1, and S_2 and K_2) on the fast scale. This approach called "CWT_Multi" in Figure 7 is hardly the only possible scheme that could be exploited. Indeed, progress in understanding river tides will require further elaboration of tidal analysis methods, and this is an area of ongoing research, as suggested by the recent progress cited above.

3.5. Contemporary Challenges

Several broad insights are evident from the above discussion of tidal methods. Tidal analysis approaches are diverse, and the complexity of nonstationary tides suggests the need for multiple analysis tools. Tidal methodology is evolving quickly, and the rate of innovation has increased dramatically in the last two decades. Rapid innovation also occurred in the 1960s and 1970s, fueled by understanding of the adverse effects of background "noise" on tidal estimates. The distinguishing factor in recent innovations has been the recognition that this apparent noise is often evidence of nonstationarity due to either physical processes [e.g., *Jay and Flinchem*, 1997; *Kukulka and Jay*, 2003a; *Buschman et al.*, 2009; *Sassi and Hoitink*, 2013] or gauge malfunctions [*Zaron and Jay*, 2014]. In the former case, the nonstationary of tidal records is useful for dynamical analyses, though it complicates tidal forecasting. Clearly, there is room for improvement in forecasting nonstationary tides, and this could be valuable for ecosystem management, habitat restoration, and navigational safety. A common thread is that constituent significance estimates used by all usual analysis approaches are less than adequate for short filter windows and strongly nonstationary data.

Another issue is the neglect of early tidal observations from circa 1830 to 1950, which often recorded only the times and heights of the two or four tidal extrema each (tidal) day [*Talke and Jay*, 2013]. These records, still rarely analyzed, are a rich source of information for understanding long-term changes in estuaries and ports [e.g., *Jay et al.*, 2011]. There is simply no good tidal analysis method, especially if the records are short (LOR<1 year) or nonstationary. Finally, we should not rule out the potential application of fundamentally different methods from other disciplines. For example, medical image analysts have the opposite problem from tidalists; medical images are so dense that there is a need to subsample optimally. Yet the fundamental question still arises: how much information is available from a certain amount of 1-D or 2-D data? Extraction of medical imaging has developed to a high level the art of linear inverse analyses from randomly sampled data [*Candès et al.*, 2006; *Candès and Romberg*, 2007]. One striking finding is that the Nyquist criterion does not directly apply to randomly sampled data, if the underlying phenomena were actually resolved in the original data set. Attempts have also been made to adapt the *Huang et al.* [1998] empirical mode decomposition to analysis of nonstationary tides, but analyses have not resulted in the isolation of coherent modes that could be interpreted in terms of tidal dynamics.

4. River Discharge-Tide Interaction

4.1. Sources of Nonlinear Interaction

The analytical models reviewed in section 2 capture only part of the dynamics that can be analyzed in full complexity using the signal processing tools discussed in section 3. Numerical models are an alternative means

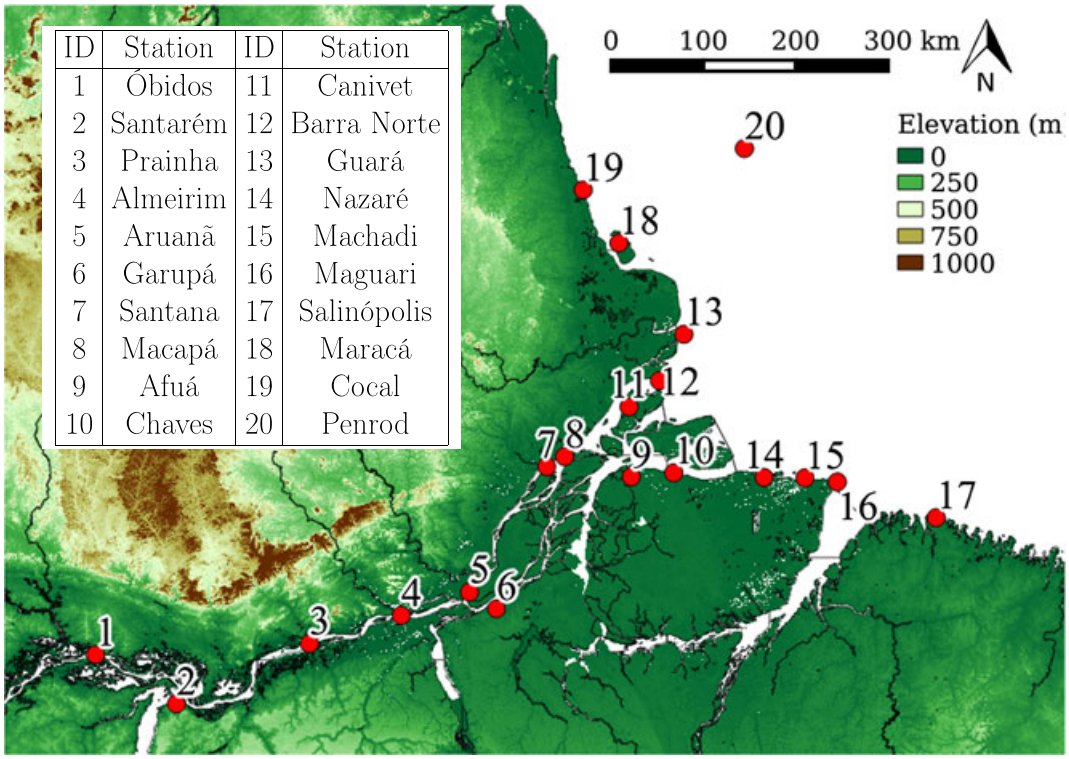

ID	Station	ID	Station
1	Óbidos	11	Canivet
2	Santarém	12	Barra Norte
3	Prainha	13	Guará
4	Almeirim	14	Nazaré
5	Aruanã	15	Machadi
6	Garupá	16	Maguari
7	Santana	17	Salinópolis
8	Macapá	18	Maracá
9	Afuá	19	Cocal
10	Chaves	20	Penrod

Figure 10. Elevation map of the Amazon tidal river basin, indicating the water level gauge stations analyzed by *Gallo and Vinzon* [2005].

of analysis, offering insight in the physical mechanisms underlying the interaction between river discharge and the tide from the governing shallow water equations [*Dronkers*, 1964]:

$$\frac{\partial U}{\partial t} + \underbrace{U\frac{\partial U}{\partial x}}_{\text{SA}} = -g\frac{\partial \zeta}{\partial x} \underbrace{-c_f \frac{U|U|}{h+\zeta}}_{\text{FR}} \tag{12}$$

$$\underbrace{\frac{\partial}{\partial x}(h+\zeta)U}_{\text{DG}} = -\frac{\partial \zeta}{\partial t} \tag{13}$$

where U is flow velocity averaged over the cross section and ζ is elevation above a horizontal reference plane. Equations (12) and (13) represent a momentum balance and a mass balance, respectively. The interaction of river discharge and the tide occurs as a result of three nonlinear terms in equations, which account for spatial acceleration (SA), friction (FR), and a gradient in the discharge (DG). Each of these terms contributes to the generation of shallow water tides, represented by angular frequencies that are sums and differences of the tides directly generated by astronomical forcing. *Parker* [1991b] offers a systematic analysis of the various nonlinear interactions among tidal constituents. In tidal rivers, the generation of M_{sf} and M_4 is particularly important, which can be illustrated by focusing on the Amazon. *Gallo and Vinzon* [2005] analyzed the contribution of each of the terms SA, FR, and DG in equations (12) and (13) to the generation of M_4 and M_{sf} in the Amazon Tidal River (Figures 10 and 11), using numerical simulations, with and without an average river discharge. The M_4 constituent is generated as a result of spatial acceleration and discharge gradients at the continental shelf and peaks at the river mouth. From there, the SA and DG contributions gradually diminish, and friction has a nearly constant contribution to the M_4 amplitudes over a distance of about 600 km. Beyond that point, SA and DG contributions have vanished and the effect of friction gradually reduces. The M_4 amplitudes reduce to zero over a region of 300 km farther inland, extending over the same river length as M_2. The M_{sf} constituent is nearly negligible at the river mouth and peaks in amplitude at about 400 km from the river mouth. At the amplitude peak of M_{sf} and farther inland, friction is the only source of nonlinearity causing the fortnightly variation.

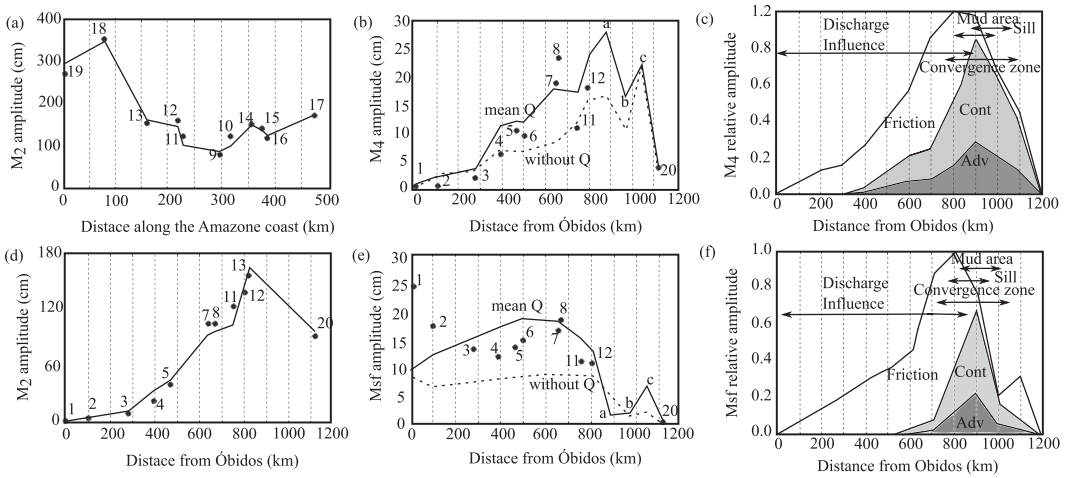

Figure 11. Tidal dynamics in the Amazon tidal river, based on *Gallo and Vinzon* [2005]. Dots are based on measurements, dashed and full lines are taken from numerical simulations. Locations of the gauge stations are indicated in Figure 10. (a) The amplitudes of the M_2 tide along the coast and in the mouth region of the Amazon, where M_2 is attenuated by the river discharge. (b) The along-river development of the main overtide, M_4. (c) The mean discharge case in Figure 11b, quantifying the relative contributions of terms representing spatial acceleration, friction, and a discharge gradient, to the development of M_4. (d and e) The along-river development of the M_2 amplitude and main subharmonic (M_{sf}), respectively. (f) The mean discharge case in Figure 11e, quantifying the relative contributions of terms representing spatial acceleration, friction, and a discharge, to the development of M_{sf}. Figures 11b and 11e also compare the development of M_4 and M_{sf} for the situation with and without a mean discharge.

Since the introduction of horizontal acoustic Doppler current profilers (H-ADCPs), the scope of field data available for tidal river analysis has widened to include continuous series of both water levels and flow velocity [*Hoitink et al.*, 2009; *Sassi et al.*, 2011a], provoking a leap forward in the range of possibilities to investigate friction effects. It allows investigation of subtidal flow processes. *Buschman et al.* [2009] solved for all terms in the subtidal momentum balance using H-ADCP velocity and surface level data at a station located about 60 km from the sea, upstream of the apex of the Berau Delta in East Kalimantan (Indonesia). This work provides field confirmation that in the upstream reaches of an estuary, the subtidal momentum equation essentially represents a balance between the surface level gradient and friction terms. The latter can be approximated using Chebyshev polynomials to simplify $U|U|$ [*Godin*, 1999]:

$$\left\langle gA\frac{\partial(h+\zeta)}{\partial x}\right\rangle + \frac{16}{15\pi}c_f W U_m^2 \left\langle \tilde{U} + 2\tilde{U}^3 \right\rangle \approx 0 \tag{14}$$

where W is channel width, A is the cross-section area, the angular brackets denote averaging over a diurnal tidal cycle, and $\tilde{U}$ is velocity made nondimensional with the maximum velocity U_m. The resulting subtidal momentum balance can be employed to further investigate the main controls on mean elevation, by starting to represent the velocity signal based on the four main species:

$$\tilde{U} \approx \tilde{U}_0 + \tilde{U}_1\cos(\omega t + \phi_1) + \tilde{U}_2\cos(2\omega t + \phi_2) + \tilde{U}_4\cos(4\omega t + \phi_4) \tag{15}$$

Buschman et al. [2009] evaluated the second term in equation 14 over a diurnal tidal cycle, which resulted in the following solution:

$$\frac{16}{15\pi}\frac{U_m^2 W c_f}{2\pi}\int_0^{2\pi}\left(\tilde{U}+2\tilde{U}^3\right)\mathrm{d}t = \frac{16U_m^2 W c_f}{15\pi}\left(\underbrace{\tilde{U}_0+2\tilde{U}_0^3}_{S_r} + \underbrace{3\left(\tilde{U}_0\tilde{U}_1^2+\tilde{U}_0\tilde{U}_2^2+\tilde{U}_0\tilde{U}_4^2\right)}_{S_{rt}}\right.$$
$$\left. + \underbrace{3\left(\tilde{U}_1^2\tilde{U}_2\cos(2\phi_1-\phi_2)+\tilde{U}_2^2\tilde{U}_4\cos(2\phi_2-\phi_4)\right)}_{S_t}\right) \tag{16}$$

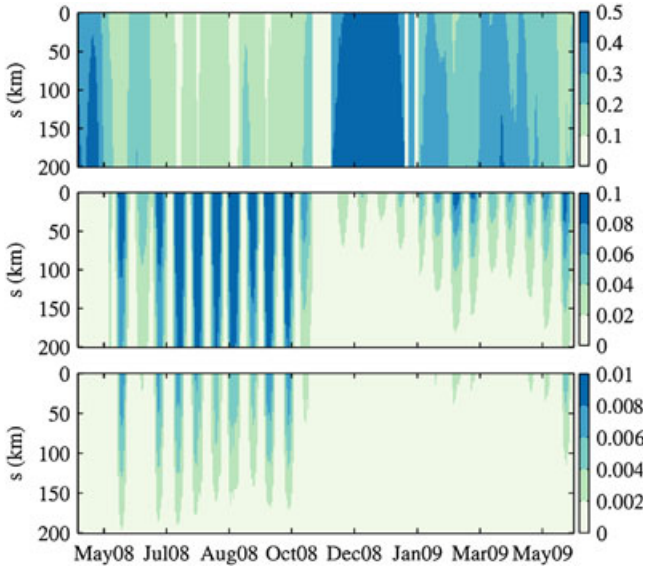

Figure 12. Dynamic contributions to subtidal friction along the Mahakam River from the (top) river flow (S_r), (middle) river discharge-tide interaction (S_{rt}), and (bottom) tidal asymmetry (S_t). For convenience, we have plotted $-S_t$, since S_t is always negative. The river mouth is at $s = 0$. Adopted from *Sassi and Hoitink* [2013].

The terms S_r, S_{rt}, and S_t highlight the contributions by residual flow (largely governed by the river discharge), river-tide interactions, and tidal asymmetry to the generation of subtidal friction (respectively), resulting in a setup of the mean waver level. The river-tide interaction term steepens the water surface profile toward the tidal river, amplifying the gradient that would occur without tides. The sign of the tidal asymmetry terms depends on the phase relations $2\phi_1 - \phi_2$ and $2\phi_2 - \phi_4$. Consequently, tidal asymmetry can amplify or partially cancel the surface level gradient.

Wavelet analysis discussed in section 3 can be employed to decompose time series of velocity into the contributions of the main tidal species, according to equation (15). These results can then be used in equation (16). Figure 12 exemplifies time series of S_r, S_{rt}, and S_t for the case of the Mahakam tidal river [*Sassi and Hoitink*, 2013]. The relative contributions of the three terms is highly dynamic, depending on the discharge. There is a high coherence between S_{rt} and $-S_t$, which implies the development, and D_4 and $D_{1/14}$ are interrelated. Variations in the contributions by river discharge-tide interaction and tidal asymmetry to the subtidal momentum balance are highly coherent.

4.2. Detiding

River discharge-tide interactions such as analyzed in the previous subsection hamper the direct estimation of terrestrial fluxes to the coastal ocean, which is important for understanding the global water, carbon, and sediment budgets. Gauges above the limit of tidal intrusion may be located as far as 1000 km from the ocean, as in the Amazon, landward of tributaries draining wet coastal regions. Discharge gauging stations at the end of the catchment, near the river mouth, generally observe water levels or flow velocity modulated by the tide. Such modulations occur at all tidal frequencies, and removing the tidal influence is a nontrivial task. The removal of the tides from a time series is known as "detiding." Detiding of stationary water level and current meter records is well established, even for data distributed in space and time, for example, collected from moving vessels [*Candela et al.*, 1992; *Foreman et al.*, 1995; *Münchow*, 2000; *Vennell and Beatson*, 2006]. For fixed-position data, the only real difference between detiding and customary HA is that detiding considers the tides to be noise, not the object of the analysis.

The hydrologic problem is different. Identifying the mean tidal properties from a HA is insufficient, as the river discharge is typically nonstationary. An accurate version of the nonstationary tide must be removed, especially if tidal fluctuations are of comparable magnitude to fluctuations due to river flow. Several studies have attempted to do this. *Lim and Lye* [2004] used a discrete wavelet transform to remove tidal influence from water level data taken 190 km from the mouth of a Malaysian River with discharge that varied between 500 and 4000 $m^3\ s^{-1}$; daily tidal influence was evident primarily during low-flow periods. A rating curve approach

was then used to estimate discharges. Because tidal properties were not specifically assessed before and after detiding, it is unclear how successful the detiding exercise was. Given the distance of the station from the mouth, it is to be expected that subtidal variations in water level would be prominent, and that these would affect discharge estimations if such fluctuations were not removed.

Pagendam and Percival [2015] compared three separate methods for detiding flow data from a small Australian River, which had river flow that varied from near zero to 500 m^3 s^{-1}. An approach that combined robust HA (for determination of the tidal properties) of flow records with Kalman-Filter smoothing applied to the detided flow time series was found to be superior to low-pass filtering and use of dynamic harmonic regression [*Young et al.*, 1999]. The latter is a method frequently used for analysis of nonstationary processes involving fewer frequencies than tidal records; it has been used for detiding of groundwater records [*Heathcote et al.*, 1997]. From a tidalists point of view, one issue with the results is the use of a stationary HA with a large number of constituents (68) for the tidal estimates based on a gappy 452 day record, which is relatively short. Because the analysis was implemented in the statistical language *R*, it is also unclear how many of the estimates would have been deemed significant in a conventional robust HA, and how realistic the tidal estimates were for low and high flows. Also, it is unclear whether subtidal variations were properly removed, or even if these oscillations were important, because the station analyzed appears to be fairly close to the ocean.

Interestingly, tidal frequencies can appear in water level records that do not stem from oceanic tidal forcing. *Briciu* [2014] used a continuous wavelet transform to demonstrate that tidal frequencies can enter hydrologic records in certain geologic circumstances, through the influence of groundwater. Variable hydropower generation (power peaking) can also result in the appearance of propagating waves, usually diel (period 24 h) of nontidal origin in tidal rivers [*Jay et al.*, 2016] and also landward of tidal influence [*Wiele and Smith*, 1996; *White et al.*, 2005; *Zolezzi et al.*, 2009]. These influences would need to be removed by detiding, if hydrologic records from such locations were to be used to estimate river flow.

4.3. Inferring River Discharge From Tidal Attenuation

It has long been known that quadratic interactions between river flow and tides affect tidal propagation in rivers [e.g., *Dronkers*, 1964]. However, *Jay and Kukulka* [2003] appear to have been the first to use fluctuations in tidal admittance at fluvial stations as a method to estimate flow, defined as the ratio of the amplitude in a tidal river, and the ocean forcing tidal amplitude. This method is the inverse of the model used by *Kukulka and Jay* [2003a], which predicted riverine tidal properties from river flow and coastal tidal amplitudes. They obtained an approximate theoretical relationship that predicts discharge from the tidal admittance. *Jay et al.* [2006] demonstrated the potential of the method to reconstruct flows from long records and estimate historic flood amplitudes, but the first analysis of errors in the method was made by *Moftakhari et al.* [2013, 2015], who reconstructed 18 d averaged and daily estimates of San Francisco Bay inflow. *Moftakhari et al.* [2015] also hindcast sediment input to San Francisco Bay. These flow and sediment input estimates were used to understand secular changes in the systems, and changes in seasonal hydrology, both important properties in understanding ecosystem trajectory. H. R. Moftakhari et al. (submitted manuscript, 2016) extended this flow estimation method to the Columbia and Fraser Rivers, demonstrating that a variety of tidal regimes and system geometries can be accommodated by the method. Probably, the largest weakness of this approach is that the *Kukulka and Jay* [2003a] model on which it is based neglects several factors (e.g., changes in salinity intrusion and system geometry) that vary with river flow and influence tidal propagation. Thus, nonphysical parameters in the model must be calibrated for each system in which it is used.

Cai et al. [2014a] use the same basic idea, i.e., that flow modulates tidal properties, and a theoretical tidal model [*Savenije et al.*, 2008; *Toffolon and Savenije*, 2011; *Cai et al.*, 2014b, 2015] to hindcast flows in the Yangtze River from tidal properties. The advantage of this approach is that a direct analytical result is achieved, so that there is no need for regression analysis to determine parameters. Still, it is necessary to fit the friction parameters to the estuary in the forward model for the tide, which is inverted to estimate discharge. Thus, parameter fitting cannot be entirely avoided. Also, the theoretical analysis used is applicable primarily to tidal channels with semidiurnal (D_2) tides. It is not applicable to estuaries with mixed diurnal-semidiurnal (D_1-D_2) tides. In summary, the idea of using the fluvial modulation of tides for hydrologic hindcasting is new and promising. The range of applicability of existing methods is unknown, not all of the mechanisms underlying the utility of the method have been explored, and no existing approach is fully satisfactory.

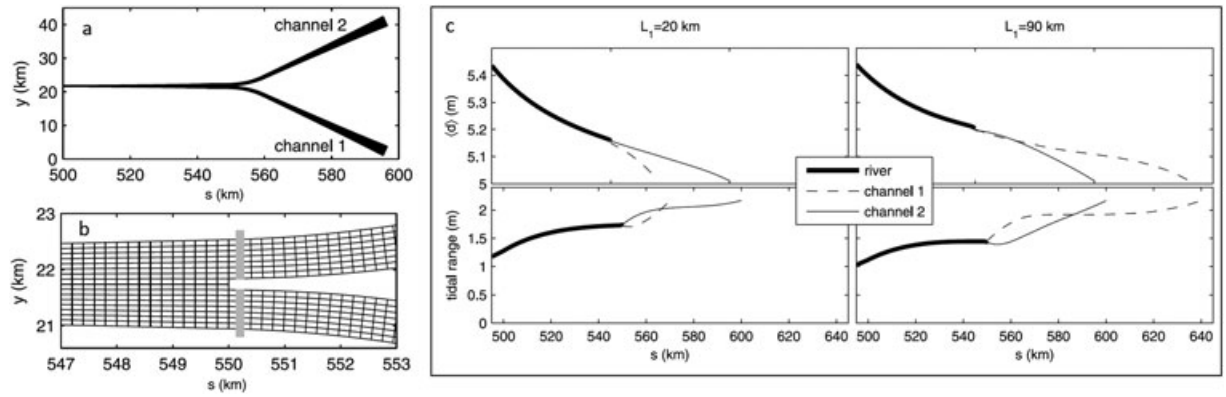

Figure 13. Idealized model of a bifurcating tidal river based on *Buschman et al.* [2010]. (a) The total mesh of the numerical model employed (b) a detail at the junction and in (c) mean depth profiles and tidal variation for a configuration in which the length of channel 1 (L_1) is shorter (left) and longer (right) than the length of channel 2 (L_2), as indicated. In both configurations, $L_2 = 50$ km.

5. Implications for Deltas

Tidal influences on the river discharge modulate the rates of sediment supply to the coastal ocean, and are a key factor controlling delta formation. The tidal motion counteracts the reduction of sediment transport capacity of a river toward the coast, shifting the deposition focus in seaward direction. River discharge-tide interactions are often active in delta channels, influencing the adjacent wetlands in terms of inundation frequency, flow velocity and sediment transport, and explaining successions found in the interdistributary deposits. This section discusses the implications of tidal river dynamics for the hydrology and geology of deltas.

5.1. Division of River Discharge Over Distributary Channels

Estuaries have often been studied with a single estuarine channel in mind, one which is connected to a river at its upstream end. Recently, *Canestrelli et al.* [2014] and *Bolla Pittaluga et al.* [2015a] showed that by considering a single channel, equilibrium bed level profiles can be derived for scenarios with a variety of forcing conditions. In many lowland areas, this view is an oversimplification of the actual anabranching planform topology, which features multiple, interconnected channels. Typically, the river discharge, sediments, nutrients, dissolved oxygen, and pollutants in a lowland river are divided between a number of branches, termed distributary channels or distributaries [e.g., *Edmonds and Slingerland*, 2008, 2010; *Sassi et al.*, 2013a]. Recent research has focused on the role of tides in the division of flow and sediment over these distributaries [*Buschman et al.*, 2010; *Sassi et al.*, 2011b; *Zhang et al.*, 2013; *Leonardi et al.*, 2015], elaborating on the concepts developed in tidal river analysis reviewed in the previous sections.

Tidal propagation in a network of channels is intrinsically more complex than in a single channel. Based on results from a linear model introduced by *Souza and Hill* [2006], *Hill and Souza* [2006] questioned whether there are preferred tidally induced Lagrangian transport pathways through tidal channel networks. Addressing this question, *Buschman et al.* [2010] developed an idealized, nonlinear model of the Berau Delta (Kalimantan, Indonesia), consisting of a river that splits in two branches that debouch in the sea (Figure 13). A constant river discharge was imposed at the upstream boundary, and a tidally varying water level at the two seaward boundaries. Length, width, and roughness were varied for the two distributary channels. The model results showed that the tide can have a significant influence on river discharge division over delta distributaries. This influence can partly be attributed to Stokes transport [*Longuet-Higgins*, 1953], which is the mean mass transport associated with a propagating wave, for which flood occurs during high water and ebb during low water. In a single-channel tidal river, the Stokes transport is typically compensated for by a Eulerian return current driven by the surface level gradient resulting from the subtidal momentum balance (equation (14)). In a multichannel system, the Stokes transport in one particular channel is not necessarily equal to the Eulerian mean return transport. This implies the mass transport generated by a progressive, or nearly progressive, tidal wave can be returned to sea by a Eulerian mean flow in a different channel. *Buschman et al.* [2010] showed that as a consequence, tides can enhance or cancel inequality in the discharge distribution that would occur in absence of the tidal motion, depending on asymmetries in distributary channel roughness, length, depth, and to a lesser degree, width.

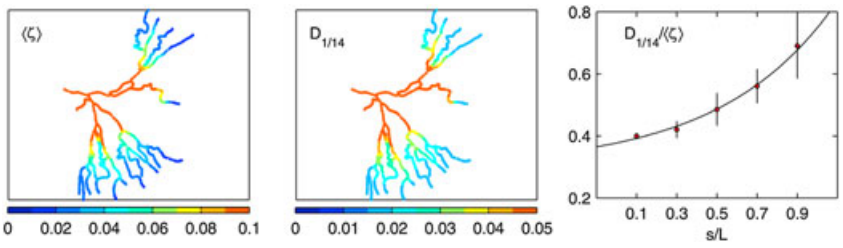

Figure 14. Resemblance between (left) mean surface elevation ($\langle\zeta\rangle$) and (middle) fortnightly tidal amplitudes ($D_{1/14}$) in the Mahakam Delta, based on *Sassi et al.* [2012a]. In both panels the color scale has been confined in order to better visualize variations toward the sea. Also shown (right) is the ratio of $D_{1/14}$ to $\langle\zeta\rangle$ as a function of normalized along-channel distance s/L, where $s = 0$ at the delta apex, i.e., the most upstream junction. L is mean distance from the apex to the sea. Circles depict the cluster means for distributaries with the similar values for s/L; the error bars denote one standard deviation.

Sassi et al. [2011b] continued the work by *Buschman et al.* [2010], using a numerical model of the Mahakam Delta (Kalimantan, Indonesia) initiated by *de Brye et al.* [2011], to show that river discharge-tide interactions can create differential water level setup in neighboring channels. The rise of the mean surface level in one channel can increase the hydraulic gradient in the neighboring channel, influencing the discharge division ratio. This mechanism favors the allocation of river discharge to smaller channels that would receive a comparatively small portion of the river discharge in absence of the tide. *Sassi et al.* [2012a] quantified the tidal influence on flow and geometrical properties of distributaries of the Mahakam Delta, which revealed a break in scaling behavior between the river-dominated and tide-dominated parts. Compared to the river-dominated part, the width convergence in the tide-dominated part is stronger and the flow velocity averaged over a diurnal tidal cycle rapidly decreases in the seaward direction. An unambiguous relation was established between mean elevation, i.e., setup, and the amplitude of the fortnightly tide $D_{1/14}$ (Figure 14). In the seaward margin of the delta where tides are dominant, the tidal motion alters the flow division increasingly more for junctions closer to the coast, up to 30% compared with a simulation without the tide.

By focusing on a distributary in the Apalachicola Delta, USA, *Leonardi et al.* [2015] suggest that even very small tides can strongly impact the velocity field at distributary mouths, irrespective of the river discharge regime. Their field results reveal that once the flow becomes unidirectional during a high-discharge event in the distributary subjected to study, tidal velocity amplitudes magnify. On the contrary, when the flow was bidirectional, increasing fluvial discharge decreased tidal velocity amplitudes down to a minimum value, reached at the limit between bidirectional and unidirectional flow. *Leonardi et al.* [2015] attribute these observations to a difference in response of the distributary system to tides. Individual branches can become resonant, or near resonant [*Alebregtse et al.*, 2013], which is one of the key phenomena in tidal channel networks that can cause ambiguous relations between flow velocity and surface elevation amplitudes. Theoretically, tides can become chaotic, which has been demonstrated for submerged channel networks in lagoons such as the Wadden Sea [*Maas*, 1997; *Maas and Doelman*, 2002]. To date, it remains unclear if delta channel networks allow such tidal behavior.

5.2. Geological Implications

Tides are one of the main factors controlling Holocene delta evolution [*Galloway*, 1975; *Orton and Reading*, 1993]. Up to the reach where tides become extinct, small-scale sedimentary structures called tidal rhythmites can preserve a hierarchy of astronomically induced tidal periods [*Kvale et al.*, 1999]. These can be retrieved from a sedimentary record using harmonic analysis in space rather than time [*Mazumder and Arima*, 2005]. Most studies aiming to interpret tidal rhythmites focus on coastal settings, yet tidal deposits can occur in inland wetlands subjected to tides at present and/or in the geological past [*Hoorn et al.*, 2010]. In river-dominated delta plains with only a minor tidal influence, the sedimentology and stratigraphic architecture can be poorly constrained, leading to simplistic depositional models of delta-plain systems based on the ancient record [*Gugliotta et al.*, 2015]. *Gugliotta et al.* [2016] aimed to decouple the seasonal fluctuations in fluvial discharge from the tidal signature in ancient deltaic deposits of the Neuquén Basin, Argentina. They show the rhythmites can be used to record variations in river discharge rather than tides, because the magnitude of river floods is stochastic and does not vary regularly, whereas tides are cyclical and relatively predictable. The recent developments in methods to process tidal signals influenced by the river discharge, as described in previous

sections, may merit the reinterpretation of sedimentary successions. The thickness of the lamina in the records may have a direct relation to tidal admittance, which relates to the river discharge.

The planform of a river delta channel network tends to be asymmetrical, and bifurcating channels commonly split their discharges unequally [*Edmonds and Slingerland*, 2007, 2008; *Bolla Pittaluga et al.*, 2015b]. Based on a numerical model simulating fluid flow, waves, sediment transport and the interaction with morphological changes, *Edmonds and Slingerland* [2008] showed that asymmetrical configurations are morphologically more stable. Morphological stability here means that the channel morphology evolves back to the initial conditions, when perturbed by adding a mound of sediment in the middle of the channel. Channel bifurcation is strongly linked to mouthbar development processes, recently reviewed by *Fagherazzi et al.* [2015]. Although it is evident that tides exert an influence on these processes, the effect of tides on bifurcation geometry and stability has rarely been addressed. Using the same process-based numerical model as *Edmonds and Slingerland* [2008], Delft3D, *Geleynse et al.* [2011] assessed the influence of tides on clastic river delta formation. They found that tide-influenced river deltas prograde mainly via lengthening of initially formed, relatively stable distributaries characterized by cyclicity in deposits, representing tidal rhythmites. The interaction between river discharge and the tide, leading to differential water level setup [*Sassi et al.*, 2011b, 2012a], may offer an explanation for the relative stability of the channels found in the results of *Geleynse et al.* [2011]. The findings of *Leonardi et al.* [2015] suggest that even in micro tidal regimes [*Pugh*, 1996], i.e., where the surface elevation amplitudes are small, velocity amplitudes can be significant even during high river discharge. This limits the number of deltas that can be considered fully fluvial dominated. Especially in branching channels, tidal surface elevation variation may poorly represent flow velocity, which has a more direct relation with sediment transport and morphology.

Avulsion can be defined as the natural process by which flow diverts out of an established river channel into a new permanent course on the adjacent floodplain [*Slingerland and Smith*, 2004]. *Jerolmack and Mohrig* [2007] found that in many lowland areas, avulsions have occurred at a distance from the coast that coincides with the backwater length, defined as a characteristic length over which the water level of the receiving basin has an influences on river hydraulics [e.g., *Te Chow*, 1959]. *Nittrouer et al.* [2012] showed that in the Mississippi River, deposition is higher in the upstream part of the backwater zone, where four major avulsions have occurred during the Holocene. *Chatanantavet et al.* [2012] then used a quasi two-dimensional morphodynamic model of a coupled river and river plume system subject to a range of water discharges to explain the causal relation between backwater length, deposition and avulsion. During low discharge, the flow decelerates in the backwater region, leading to deposition, which can divert the flow out of the river channel. During high discharge, a drawdown occurs and the flow accelerates and has a capacity to remove deposits, reducing the propensity for avulsion at locations closer to the receiving basin (Figure 15). The near-coastal area can be a zone of erosion, dominated by high-flow events [*Lamb et al.*, 2012]. The mean water level setup created by the interaction between river discharge and tides has a direct effect on mean surface level profiles, which accumulates in the upstream direction (e.g., Figure 13). The calculations performed to obtain the surface level profiles in Figure 15 have, however, considered only S_r, and neglect S_{rt} and S_t in the subtidal momentum balance (equations 14 and 16). This can only be justified in rivers with small tidal velocity amplitudes, which are not easily estimated from surface elevation amplitudes. Given the results of *Leonardi et al.* [2015], these terms should be included.

5.3. Links With Salinity Intrusion and Wetland Research

The transition between land and sea can be considered among the most complex regions on Earth, because of the interaction of numerous physical, chemical, and biological processes [*Dalrymple and Choi*, 2007; *Schwartz*, 2005]. In tidal rivers and the adjacent wetlands, fluxes of organic and inorganic particles and dissolved substances such as carbon, nitrogen, and phosphorus vary at tidal frequencies, complicating these interactions. *Ensign et al.* [2012, 2013, 2014a, 2014b] argue that hydrologic and geomorphologic processes by which tides affect river channel and riparian morphology within the tidal freshwater zone are insufficiently understood to predict the fate of tidal rivers and wetlands, in an era of anthropogenic changes including sea level rise. Downstream of the tidal freshwater zone, the effect of sea level rise is reinforced by sinking of deltas due to mineral and water extraction, reduced sediment input, and floodplain engineering [*Syvitski et al.*, 2009]. The forcing functions of tidal rivers are thus in state of continual change. In general, tidal rivers are expected to become deeper when deltas are sinking, which amplifies the tidal motion and promotes salinity intrusion.

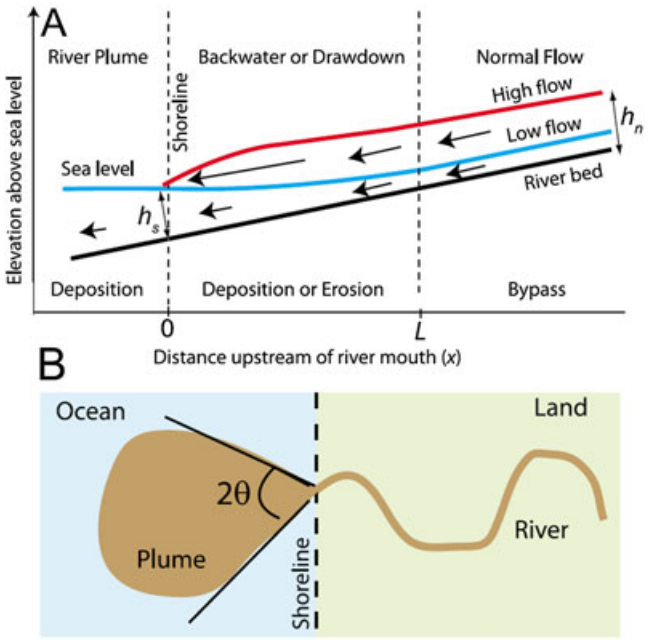

Figure 15. Cartoon showing a river entering an ocean with three zones of interest: a normal flow area, where depth is constant along the channel, a transition zone where mean sea level influences river depth, and the offshore river plume in (a) cross section and (b) plan view. At low flow, the transitional region is a zone of backwater, where the water depth at the shoreline (h_s) is greater than the normal flow depth (h_n), and the water surface (blue) and bed (black) diverge downstream, resulting in deceleration (shown by length of arrows) and deposition. At high flow $h_n > h_s$, the water surface (red) is convex, resulting in spatial acceleration of flow and erosion. In both cases, the elevation of the water surface at the river mouth is relatively insensitive to discharge due to lateral spreading of the plume. Adopted from *Lamb et al.* [2012], after *Lane* [1957].

Consequently, the geographic location of the tidal freshwater zone shifts inland. The remainder of this section will address recent approaches to analysis of salinity intrusion and the possibilities of multiscale modeling and monitoring of tidal rivers and wetlands.

The analytical models referred to in section 2 offer simple tools that can be used to investigate how both the tidal motion and salinity intrusion responds to sea level rise and channel deepening in a single channel [*Cai et al.*, 2012]. In branching channels, salinity intrusion can only be partly captured in a one-dimensional channel network model [*Zhang et al.*, 2012b] that can represent Stokes transport [*Buschman et al.*, 2010] and Eulerian residual transport driven by differential water level setup [*Sassi et al.*, 2011b] but fails to properly model exchange processes at the connections between channels. Recent field observations show that salinity exchange at tidal channel junctions may depend on three-dimensional aspects of the flow, caused by flow curvature and abrupt changes in the character of the tide apparent from the phase difference between water level and flow velocity variation [*Buschman et al.*, 2013]. In the Yangtze Delta, a relatively narrow, shallow channel draws saline water into the main river branch at a junction located about 100 km from the river mouth [*Xue et al.*, 2009]. Differences in the length and depth along alternative pathways from a channel junction to the sea can result in marked differences in the character of the tide in neighboring branches, which then govern the limit of salinity intrusion [*Buschman et al.*, 2013; *Lu et al.*, 2015].

Jay et al. [2015] showed how the regression models described in section 2 can directly be used to quantify the roles of tides, river flow, hydropower operations, and wind forcing in determining water levels in the lower Columbia River and its floodplain wetlands, providing a 21 year inundation hindcasts. This was further illustrated by *Jay et al.* [2016], who also revealed the system zones established from analysis of water level records reflect geological features and coincide with wetland vegetation zones. Regression models offer a straightforward means of monitoring the main factors controlling inundation statistics, which are key to wetland functioning. It is likely they are outperformed by artificial neural network models in terms of skill scores [e.g., *Hidayat et al.*, 2014] but provide insight into the underlying processes.

Data with spatial coverage can complement such data-driven approach. Among the available remote sensing options [e.g., *Ozesmi and Bauer*, 2002], synthetic aperture radar (SAR) may be particularly suitable, as it detects water under vegetation and can be used to create flood occurrence maps in densely forested wetlands [*Romshoo*, 2004; *Henderson and Lewis*, 2008; *Hoekman*, 2009; *Hidayat et al.*, 2012; *Kim et al.*, 2014]. It is possible to evaluate water surface slope with Spaceborne Interferometric SAR [*Sun et al.*, 2003], but this procedure has not become common.

Numerical models simulating hydrodynamics, sediment transport, and morphodynamics are in a phase of rapid developments toward generic tools that may address the needs in the context of tidal wetland restoration and taking measures to cope with climate change. Flexible meshes accommodate the land-sea continuum in models stretching from deep water (>100 m) up until the upstream limit of the tidal river [e.g., *Hervouet*, 2007; *Twigt et al.*, 2009; *de Brye et al.*, 2010; *Canestrelli et al.*, 2010; *de Brye et al.*, 2011]. Resolution flexibility captures the multiscale nature of the nonlinear development of a tidal wave propagating from deep water into a tidal river. For example, the horizontal mesh resolution of the model by *de Brye et al.* [2010], later used by *Pham Van et al.* [2016, 2015], decreases from 10 km in the coastal ocean to 100 m in the upper reaches of the tidal river. Finite element and finite-volume numerical methods are well established for hydrodynamic modeling purposes, yet it is only recently that such models have become a realistic option without having recourse to a high performance computing facility. One of the main difficulties of simulating hydrologic and geomorphologic processes in tidal wetlands is wetting and drying of cells [*D'Alpaos and Defina*, 2007]. Using a finite-volume model referred to as Delft3D Flexible Mesh [*Kernkamp et al.*, 2011] in a 2-D mode, *Achete et al.* [2015] took a first step toward the modeling of sediment dynamics and the associated ecological parameters in the San Francisco tidal wetlands. Flexible mesh numerical models have the promise to reproduce sediment transport in tidal rivers and the adjacent wetlands from source to sink [*Pham Van et al.*, 2015; *Achete et al.*, 2015] and to allow coupling between processes governing flow, sediment transport, morphology, and ecology over a range of spatial and temporal scales.

6. Conclusions

Predicting the fate of tidal rivers and the adjacent wetlands in response to contemporary threats including sea level rise and sinking of deltas will likely remain a challenge for the decades to come. Advanced methods of analysis are available based on a wide variety signal processing techniques and mechanistic understanding of river discharge-tide interactions. Characteristic phenomena in tidal freshwater rivers include tidal bores, fortnightly tides, and water level setup that raises the mean surface levels above the backwater and drawdown profiles that would occur in absence of tides. Analytical models can capture tidal long-wave propagation under the influence of river discharge. Empirical models are available to predict tidal river surface levels from river discharge and conditions at sea, using a number of gauge stations along the tidal river as input for parameter estimation. Knowledge of the interactions between river discharge and tides has yielded methods to remove the tidal influence from data series at near-coastal stations and to estimate terrestrial fluxes to the coastal ocean. Historical estimates of river discharge can be inferred from the ratio between tidal amplitudes at sea and in the tidal river, i.e., the tidal admittance. Tidal admittance may also be reflected in depositional patterns termed tidal rhythmites, which offers the possibility of retrieving discharge estimates from geological records.

In branching tidal channels, the tidal motion can induce a residual flow in response to geometrical differences between branches and bed roughness variation. At river bifurcations subject to tides, differential water level setup from nonlinear interaction between river discharge and the tides tends to cancel the inequality in the division of river discharge over distributary channels. Tidal velocity amplitudes in distributary channels cannot readily be estimated from tidal elevation amplitudes, because of reflection of tidal energy and the possibility of (near) resonance behavior. The tidal motion may act to reduce the asymmetric division of discharge and sediment over distributary channels and explain the planform stability of mixed river-tide-dominated deltas. The setup of water levels in a tidal river accumulates in the upstream direction up to the point of tidal extinction and may influence a river's propensity to avulse. Dissimilarities between the geometry of branching tidal channels may cause differences in tidal behavior between the channels. Tidal phase differences between interconnected channels and flow curvature can cause a complex flow structure at channel junctions and marked differences in salinity intrusion between channels.

Multidisciplinary tidal river research addresses multiple contemporary challenges. Delta plains hosting tidal rivers represent regions where the effects of global warming on sea level and discharge are focused. Human measures to mitigate hazards of flood, drought, and loss of biodiversity add to the factors that keep tidal rivers in a state of flux. Joint efforts linking knowledge from hydrology, physical oceanography, and geology are needed to obtain a sharper view on the changes in hydrodynamic and sedimentary tidal regimes, and the associated geomorphological adaptations. Concrete research priorities for the coming decade are threefold. First, there are too few analyses available focused on the interpretation of long-term water level records in tidal rivers. For many river harbors, the records go back in time at least for a century. In conjunction with hindcasts of the river discharge and ocean tidal amplitudes, historical analyses of harbor tides can reveal natural and anthropogenic trends in tidal river dynamics and possible regime changes. Second, there is a lack of knowledge about bedform dynamics in tidal rivers, which cause spatial and temporal variation in the flow resistance factor c_f used throughout this manuscript. In particular, the development of dunes in tidal rivers where the sediment characteristics transition from sand to mud needs to be better understood. New techniques for in situ monitoring [e.g., *Sassi et al.*, 2012b, 2013b; *Vermeulen et al.*, 2011, 2013, 2014] can assist further exploration of the associated processes governing flow and sediment transport. Third, research on the interaction between tidal river hydrodynamics and wetland vegetation deserves priority. Wetland restoration programs and climate change adaptation efforts in deltas can directly benefit from such analyses.

Glossary

avulsion: Natural process by which flow diverts out of an established river channel into a new permanent course on the adjacent floodplain

clastic: Clastic material is composed of clasts, which are fragments of weathered or eroded rock.

debouch: The word "bouche" means mouth in French. A river debouches in the coastal ocean where the mouth of the river is.

Greenwich phases: Greenwich phases of the tidal motion adopt 0.00 h 1 January 1900, Greenwich Mean Time, as a time reference.

$D_{1/14}$, D_1, D_2, and D_4: Variation of amplitudes and phases of the fortnighly, diurnal, semidiurnal, and quarterdiurnal tides can either be represented by a large number of tidal constituents or by amplitudes and phase variation of lumped harmonics termed $D_{1/14}$, D_1, D_2, and D_4 (respectively).

head of the tide: tidal limit or the most upstream location where a river is affected by tidal fluctuations.

K_1: Principal diurnal tidal constituent with solar and lunar contributions.

LOR: length of record. The number of tidal constituents that can be resolved increases with the LOR.

M_2: Principal lunar semidiurnal tidal constituent.

M_{sf}: Lunisolar synodic fortnightly tidal constituent.

N_2: Larger elliptical lunar semidiurnal tidal constituent.

O_1: Principal lunar diurnal tidal constituent.

P_1: Solar diurnal tidal constituent.

Q_1: Larger elliptical lunar diurnal tidal constituent.

S_2: Principal solar semidiurnal tidal constituent.

subtidal: Refers to low-frequency oscillations, with periods significantly larger than 1 day.

tidal constituents: Sinusoidal waves with frequencies determined from astronomical and hydrodynamic theory, whose amplitudes and phases are determined by least squares regression analysis.

tidal rythmite: A tidal rhythmite consists of layers of sediment or sedimentary rock featuring a periodicity related to the tidal motion.

tidal species: Group of tidal constituents with similar frequencies.

tributary: Stream or river feeding the main stem in a drainage basin.

whelp: Secondary wave superimposed on a solitary wave such as a tidal bore, which can be observed by eye as an undulation of the water surface.

Acknowledgments
Internal Portland State University funds and Tierra Solutions, Inc. (contract PSU_002_0) provided support for D. A. Jay for preparation of this review. We thank Pascal Matte for the data used in Figure 9, and Merel Verbeek, Karl Kästner, Bart Vermeulen, and Victor Bense for their contributions to this manuscript. This study has been supported by the Netherlands Organization for Scientific Research (NWO), project 1022/01966/ALW, and by the Royal Netherlands Academy of Arts and Sciences (KNAW), project SPIN3-JRP-29. Data used in Figure 8 can be obtained by sending an email to the corresponding author (Ton.Hoitink@wur.nl).

References

Achete, F., M. van der Wegen, D. Roelvink, and B. Jaffe (2015), A 2-d process-based model for suspended sediment dynamics: A first step towards ecological modeling, *Hydrol. Earth Syst. Sci.*, *19*, 2837–2857, doi:10.5194/hess-19-2837-2015.
Alebregtse, N. C., H. De Swart, and H. Schuttelaars (2013), Resonance characteristics of tides in branching channels, *J. Fluid Mech.*, *728*, R3.
Aubrey, D., and P. Speer (1985), A study of non-linear tidal propagation in shallow inlet/estuarine systems part I: Observations, *Estuarine Coastal Shelf Sci.*, *21*(2), 185–205.
Barendregt, A., and C. Swarth (2013), Tidal freshwater wetlands: Variation and changes, *Estuaries Coasts*, *36*(3), 445–456.
Benjamin, T., and M. Lighthill (1954), On cnoidal waves and bores, *Proc. R. Soc. A*, *224*(1159), 448–460.
Bolla Pittaluga, M., N. Tambroni, A. Canestrelli, R. Slingerland, S. Lanzoni, and G. Seminara (2015a), Where river and tide meet: The morphodynamic equilibrium of alluvial estuaries, *J. Geophys. Res. Earth Surf.*, *120*, 75–94, doi:10.1002/2014JF003233.
Bolla Pittaluga, M., G. Coco, and M. G. Kleinhans (2015b), A unified framework for stability of channel bifurcations in gravel and sand fluvial systems, *Geophys. Res. Lett.*, *42*(18), 7521–7536.
Bonneton, N., P. Bonneton, J.-P. Parisot, A. Sottolichio, and G. Detandt (2012), Tidal bore and Mascaret–Example of Garonne and Seine Rivers [Ressaut de marée et Mascaret - Exemples de la Garonne et de la Seine], *C. R. Geosci.*, *344*(10), 508–515, doi:10.1016/j.crte.2012.09.003.
Bonneton, P., N. Bonneton, J.-P. Parisot, and B. Castelle (2015), Tidal bore dynamics in funnel-shaped estuaries, *J. Geophys. Res. Oceans*, *120*, 923–941, doi:10.1002/2014JC010267.
Briciu, A. E. (2014), Wavelet analysis of lunar semidiurnal tidal influence on selected inland rivers across the globe, *Sci. Rep.*, *4*, 4193.
Buschman, F. A., A. J. F. Hoitink, M. Van Der Vegt, and P. Hoekstra (2009), Subtidal water level variation controlled by river flow and tides, *Water Resour. Res.*, *45*, W10420, doi:10.1029/2009WR008167.
Buschman, F. A., A. J. F. Hoitink, M. Van Der Vegt, and P. Hoekstra (2010), Subtidal flow division at a shallow tidal junction, *Water Resour. Res.*, *46*, W12515, doi:10.1029/2010WR009266.
Buschman, F. A., M. V. D. Vegt, A. J. F. Hoitink, and P. Hoekstra (2013), Water and suspended sediment division at a stratified tidal junction, *J. Geophys. Res. Oceans*, *118*, 1459–1472, doi:10.1002/jgrc.20124.
Cai, H., H. H. G. Savenije, and M. Toffolon (2012), A new analytical framework for assessing the effect of sea-level rise and dredging on tidal damping in estuaries, *J. Geophys. Res.*, *117*, C09023, doi:10.1029/2012JC008000.
Cai, H., H. H. G. Savenije, and C. Jiang (2014a), Analytical approach for predicting fresh water discharge in an estuary based on tidal water level observations, *Hydrol. Earth Syst. Sci.*, *18*(10), 4153–4168.
Cai, H., H. Savenije, and M. Toffolon (2014b), Linking the river to the estuary: Influence of river discharge on tidal damping, *Hydrol. Earth Syst. Sci.*, *18*(1), 287–304, doi:10.5194/hess-18-287-2014.
Cai, H., H. H. G. Savenije, C. Jiang, L. Zhao, and Q. Yang (2015), Analytical approach for determining the mean water level profile in an estuary with substantial fresh water discharge, *Hydrol. Earth Syst. Sci. Discuss.*, *12*(8), 8381–8417.
Cameron, W. M., and D. W. Pritchard (1963), The sea: Ideas and observations on progress in the study of the seas, in *The Composition of Sea-Water, Comparative and Descriptive Oceanography*, Wiley-Interscience, New York, 306–324.
Candela, J., R. C. Beardsley, and R. Limeburner (1992), Separation of tidal and subtidal currents in ship-mounted acoustic doppler current profiler observations, *J. Geophys. Res.*, *97*(C1), 769–788.
Candès, E., and J. Romberg (2007), Sparsity and incoherence in compressive sampling, *Inverse Problems*, *23*(3), 969, doi:10.1088/0266-5611/23/3/008.
Candès, E. J., J. Romberg, and T. Tao (2006), Robust uncertainty principles: Exact signal reconstruction from highly incomplete frequency information, *IEEE Trans. Inf. Theory*, *52*(2), 489–509.
Canestrelli, A., S. Fagherazzi, A. Defina, and S. Lanzoni (2010), Tidal hydrodynamics and erosional power in the Fly River delta, Papua New Guinea, *J. Geophys. Res.*, *115*, F04033, doi:10.1029/2009JF001355.
Canestrelli, A., S. Lanzoni, and S. Fagherazzi (2014), One-dimensional numerical modeling of the long-term morphodynamic evolution of a tidally-dominated estuary: The Lower Fly River (Papua New Guinea), *Sediment. Geol.*, *301*, 107–119.
Cartwright, D. E. (1968), A unified analysis of tides and surges round North and East Britain, *Philos. Trans. R. Soc. A*, *263*(1134), 1–55.
Cartwright, D. E., and R. J. Tayler (1971), New computations of the tide-generating potential, *Geophys. J. Int.*, *23*(1), 45–73.
Caspers, H. (1967), Estuaries, in *Estuaries: Analysis of Definitions and Biological Considerations*, Am. Assoc. Adv. Sci. Publ. 83, Washington, D. C., 6–8.
Chanson, H. (2009), Current knowledge on hydraulic jumps and related phenomena: A survey of experimental results, *Eur. J. Mech. B/Fluids*, *28*(2), 191–210, doi:10.1016/j.euromechflu.2008.06.004.
Chatanantavet, P., M. P. Lamb, and J. A. Nittrouer (2012), Backwater controls of avulsion location on deltas, *Geophys. Res. Lett.*, *39*, L01402, doi:10.1029/2011GL050197.
Codiga, D. L. (2011), Unified tidal analysis and prediction using the UTide Matlab functions, *GSO Tech. Rep. 2011-01*, Graduate School of Oceanography, Univ. of Rhode Island Narragansett, RI.
D'Alpaos, L., and A. Defina (2007), Mathematical modeling of tidal hydrodynamics in shallow lagoons: A review of open issues and applications to the Venice lagoon, *Comput. Geosci.*, *33*(4), 476–496.
Dalrymple, R. W., and K. Choi (2007), Morphologic and facies trends through the fluvial-marine transition in tide-dominated depositional systems: A schematic framework for environmental and sequence-stratigraphic interpretation, *Earth Sci. Rev.*, *81*(3), 135–174.
Darwin, G. H. (1893), On an apparatus for facilitating the reduction of tidal observations, *Proc. R. Soc. A*, *52*, 345–389.
Day, J. W., C. A. S. Hall, W. M. Kemp, and A. Yáñez-Arancibia (1989), *Estuarine Ecology*, John Wiley, New York.
de Brye, B., A. de Brauwere, O. Gourgue, T. Kärnä, J. Lambrechts, R. Comblen, and E. Deleersnijder (2010), A finite-element, multi-scale model of the Scheldt tributaries, river, estuary and ROFI, *Coastal Eng.*, *57*(9), 850–863.
de Brye, B., S. Schellen, M. Sassi, B. Vermeulen, T. Kärnä, E. Deleersnijder, and T. Hoitink (2011), Preliminary results of a finite-element, multi-scale model of the Mahakam delta (Indonesia), *Ocean Dyn.*, *61*(8), 1107–1120.
Dohler, G. (1964), Tides in Canadian waters, *Tech. Rep.*, Can. Hydrogr. Serv., Mar. Sci. Branch, Ottawa.
Doodson, A. (1957), *The Analysis and Prediction of Tides in Shallow Water*, vol. 41, Int. Hydrogr. Bureau, Univ. of Calif.
Doodson, A. T. (1921), The harmonic development of the tide-generating potential, *Proc. R. Soc. A*, *100*, 305–329.
Doodson, A. T. (1956), Tides and storm surges in a long uniform gulf, *Proc. R. Soc. A*, *A237*, 325–343.
Dorrestein, R. (1961), *Amplification of Long Waves in Bays*, Florida Engineering and Industrial Experiment Station, 213 pp., Univ. of Calif.
Dronkers, J. J. (1964), *Tidal Computations in Rivers and Coastal Waters*, North-Holland Publ. Comp., Amsterdam.
Dyer, K. (1997), *Estuaries: A Physical Introduction*, 195 pp., Wiley, Univ. of Wisconsin–Madison.
Edmonds, D. A., and R. L. Slingerland (2007), Mechanics of river mouth bar formation: Implications for the morphodynamics of delta distributary networks, *J. Geophys. Res.*, *112*, F02034, doi:10.1029/2006JF000574.

Edmonds, D. A., and R. L. Slingerland (2008), Stability of delta distributary networks and their bifurcations, *Water Resour. Res.*, *44*, W09426, doi:10.1029/2008WR006992.
Edmonds, D. A., and R. L. Slingerland (2010), Significant effect of sediment cohesion on delta morphology, *Nat. Geosci.*, *3*(2), 105–109.
Elliott, M., and D. S. McLusky (2002), The need for definitions in understanding estuaries, *Estuarine Coastal Shelf Sci.*, *55*(6), 815–827.
Ensign, S. H., G. B. Noe, C. R. Hupp, and S. Fagherazzi (2012), A meeting of the waters: Interdisciplinary challenges and opportunities in tidal rivers, *Eos Trans. AGU*, *93*(45), 455–456.
Ensign, S. H., M. W. Doyle, and M. F. Piehler (2013), The effect of tide on the hydrology and morphology of a freshwater river, *Earth Surf. Processes Landforms*, *38*(6), 655–660.
Ensign, S. H., C. R. Hupp, G. B. Noe, K. W. Krauss, and C. L. Stagg (2014a), Sediment accretion in tidal freshwater forests and oligohaline marshes of the Waccamaw and Savannah Rivers, USA, *Estuaries Coasts*, *37*(5), 1107–1119.
Ensign, S. H., G. B. Noe, and C. R. Hupp (2014b), Linking channel hydrology with riparian wetland accretion in tidal rivers, *J. Geophys. Res. Earth Surf.*, *119*, 28–44, doi:10.1002/2013JF002737.
Fagherazzi, S., D. A. Edmonds, W. Nardin, N. Leonardi, A. Canestrelli, F. Falcini, D. J. Jerolmack, G. Mariotti, J. C. Rowland, and R. L. Slingerland (2015), Dynamics of river mouth deposits, *Rev. Geophys.*, *53*, 642–672, doi:10.1002/2014RG000451.
Fairbridge, R. W. (1980), The Estuary: Its Definition and Geodynamic Cycle, in *Chemistry and Biogeochemistry of Estuaries*, Wiley, New York.
Favre, H. (1935), *Etude théorique et expérimentale des ondes de translation dans les canaux découverts*, Dunod, Paris, France.
Flinchem, E., and D. Jay (2000), An introduction to wavelet transform tidal analysis methods, *Estuarine Coastal Shelf Sci.*, *51*(2), 177–200.
Foreman, M. (1977), Manual for tidal heights analysis and prediction, *Tech. Rep.*, Sidney, B. C.
Foreman, M., J. Cherniawsky, and V. Ballantyne (2009), Versatile harmonic tidal analysis: Improvements and applications, *J. Atmos. Oceanic Technol.*, *26*(4), 806–817.
Foreman, M. G., W. R. Crawford, and R. F. Marsden (1995), De-tiding: Theory and practice, in *Quantitative Skill Assessment for Coastal Ocean Models*, pp. 203–239, AGU, Washington, D. C.
Friedrichs, C., and D. Aubrey (1994), Tidal propagation in strongly convergent channels, *J. Geophys. Res.*, *99*(C2), 3321–3336, doi:10.1029/93JC03219.
Friedrichs, C., and O. Madsen (1992), Nonlinear diffusion of the tidal signal in frictionally dominated embayments, *J. Geophys. Res.*, *97*(N3C4), 5637–5650.
Frison, T. W., H. D. Abarbanel, M. D. Earle, J. R. Schultz, and W. D. Scherer (1999), Chaos and predictability in ocean water levels, *J. Geophys. Res.*, *104*(C4), 7935–7951.
Gallo, M. N., and S. B. Vinzon (2005), Generation of overtides and compound tides in Amazon estuary, *Ocean Dyn.*, *55*(5–6), 441–448.
Galloway, W. E. (1975), Deltas: Models for exploration, in *Process Framework for Describing the Morphologic and Stratigraphic Evolution of Deltaic Depositional Systems*, Houston Geol. Soc., Houston, Texas, 87–98.
Geleynse, N., J. E. Storms, D.-J. R. Walstra, H. A. Jagers, Z. B. Wang, and M. J. Stive (2011), Controls on river delta formation; insights from numerical modelling, *Earth Planet. Sci. Lett.*, *302*(1), 217–226.
Geyer, W. R., and G. C. Kineke (1995), Observations of currents and water properties in the Amazon frontal zone, *J. Geophys. Res.*, *100*(C2), 2321–2339.
Godin, G. (1972), *The Analysis of Tides*, Univ. of Toronto Press, Toronto, Buffalo.
Godin, G. (1983), On the predictability of currents, *Int. Hydrogr. Rev.*, *60*, 119–126.
Godin, G. (1991a), Frictional effects in river tides, *Tidal Hydrodyn.*, *379*, 402.
Godin, G. (1991b), Compact approximations to the bottom friction term, for the study of tides propagating in channels, *Cont. Shelf Res.*, *11*(7), 579–589.
Godin, G. (1999), The propagation of tides up rivers with special considerations on the upper Saint Lawrence River, *Estuarine Coastal Shelf Sci.*, *48*(3), 307–324.
Green, G. (1838), On the motion of waves in a variable canal of small depth and width, *Trans. Cambridge Philos. Soc.*, *6*, 457.
Gugliotta, M., S. S. Flint, D. M. Hodgson, and G. D. Veiga (2015), Stratigraphic record of river-dominated crevasse subdeltas with tidal influence (Lajas formation, Argentina), *J. Sediment. Res.*, *85*(3), 265–284.
Gugliotta, M., C. E. Kurcinka, R. W. Dalrymple, S. S. Flint, and D. M. Hodgson (2016), Decoupling seasonal fluctuations in fluvial discharge from the tidal signature in ancient deltaic deposits: An example from the Neuquén Basin, Argentina, *J. Geol. Soc.*, *173*(1), 94–107.
Guilcher, A. (1958), *Coastal and submarine morphology: Methuen and Co.*, Methuen and Co., London.
Guo, L., M. van der Wegen, D. A. Jay, P. Matte, Z. B. Wang, D. Roelvink, and Q. He (2015), River-tide dynamics: Exploration of nonstationary and nonlinear tidal behavior in the Yangtze River estuary, *J. Geophys. Res. Oceans*, doi:10.1002/2014JC010491.
Heathcote, J., R. Lewis, D. Russell, and R. Soley (1997), Cardiff bay barrage: Investigating groundwater control in a tidal aquifer, *Q. J. Eng. Geol. Hydrogeol.*, *30*(1), 63–77.
Henderson, F. (1966), *Open Channel Flow*, MacMi1lan, New York.
Henderson, F. M., and A. J. Lewis (2008), Radar detection of wetland ecosystems: A review, *Int. J. Remote Sens.*, *29*(20), 5809–5835.
Hervouet, J.-M. (2007), *Hydrodynamics of Free Surface Flows: Modelling With the Finite Element Method*, John Wiley, Chichester, U. K.
Hidayat, H. (2013), Runoff, discharge and flood occurrence in a poorly gauged tropical basin: The Mahakam River, Kalimantan, PhD thesis, Hydrology and Quantitative Water Management Group, Department of Environmental Sciences, Wageningen Univ.
Hidayat, H., D. H. Hoekman, M. A. M. Vissers, and A. J. F. Hoitink (2012), Flood occurrence mapping of the middle Mahakam lowland area using satellite radar, *Hydrol. Earth Syst. Sci.*, *16*(7), 1805–1816.
Hidayat, H., A. Hoitink, M. Sassi, and P. Torfs (2014), Prediction of discharge in a tidal river using artificial neural networks, *J. Hydrol. Eng.*, *19*(8), 4014006.
Hill, A. E., and A. J. Souza (2006), Tidal dynamics in channels: 2. Complex channel networks, *J. Geophys. Res.*, *111*, C11021, doi:10.1029/2006JC003670.
Hoekman, D. H. (2009), *Monitoring Tropical Peat Swamp Deforestation and Hydrological Dynamics by ASAR and PALSAR, Geosci. and Remote Sens.*, edited by Pei-Gee Peter Ho, InTech, doi:10.5772/8288.
Hoitink, A. J. F., P. Hoekstra, and D. S. Van Maren (2003), Flow asymmetry associated with astronomical tides: Implications for the residual transport of sediment, *J. Geophys. Res.*, *108*(C10), 3315, doi:10.1029/2002JC001539.
Hoitink, A. J. F., F. A. Buschman, and B. Vermeulen (2009), Continuous measurements of discharge from a horizontal acoustic doppler current profiler in a tidal river, *Water Resour. Res.*, *45*, W11406, doi:10.1029/2009WR007791.
Hoorn, C., F. P. Wesselingh, J. Hovikoski, and J. Guerrero (2010), The development of the Amazonian mega-wetland (Miocene; Brazil, Colombia, Peru, Bolivia), in *Amazonia: Landscape and Species Evolution: A Look into the Past*, pp. 123–142, Blackwell-Wiley, Hoboken, N. J.
Horrevoets, A., H. Savenije, J. Schuurman, and S. Graas (2004), The influence of river discharge on tidal damping in alluvial estuaries, *J. Hydrol.*, *294*(4), 213–228.

Huang, N. E., Z. Shen, S. R. Long, M. C. Wu, H. H. Shih, Q. Zheng, N.-C. Yen, C. C. Tung, and H. H. Liu (1998), The empirical mode decomposition and the Hilbert spectrum for nonlinear and non-stationary time series analysis, *Proc. R. Soc. A*, *454*, 903–995, The Royal Society.
Hunt, J. (1964), Tidal oscillations in estuaries, *Geophys. J. Int.*, *8*(4), 440–455.
International Hydrographic Organization (1994), *Hydrographic Dictionary, Part I, English*, 5th ed., 280 pp., Special Publication N. 32, Monaco.
Jay, D. A. (1991), Progress in Tidal Hydrodynamics, in *Internal Asymmetry and Anharmonicity in Estuarine Flows*, pp. 521–543., John Wiley, N. J.
Jay, D. A. (1997), Super-resolution of tides revisited, in *Fifth Annual Meeting of The Oceanography Society Meeting*, The Oceanography Society, Rockville.
Jay, D. A., and E. P. Flinchem (1997), Interaction of fluctuating river flow with a barotropic tide: A demonstration of wavelet tidal analysis methods, *J. Geophys. Res.*, *102*(C3), 5705–5720.
Jay, D. A., and E. P. Flinchem (1999), A comparison of methods for analysis of tidal records containing multi-scale non-tidal background energy, *Cont. Shelf Res.*, *19*(13), 1695–1732.
Jay, D. A., and T. Kukulka (2003), Revising the paradigm of tidal analysis-the uses of non-stationary data, *Ocean Dyn.*, *53*(3), 110–125.
Jay, D. A., B. S. Giese, and C. R. Sherwood (1990), Energetics and sedimentary processes in the Columbia River estuary, *Prog. Oceanogr.*, *25*(1), 157–174.
Jay, D. A., R. E. Flick, and T. Kukulka (2006), A long-term San Francisco Bay inflow record derived from tides: Defining the great flood of 1862, Abstract #GC13B-1228 presented at Fall Meeting, vol. 1, 1228 pp., AGU, San Francisco, Calif.
Jay, D. A., K. Leffler, and S. Degens (2011), Long-term evolution of Columbia River tides, *J. Waterw. Port Coastal Ocean Eng.*, *137*(4), 182–191.
Jay, D. A., K. Leffler, H. L. Diefenderfer, and A. B. Borde (2015), Tidal-fluvial and estuarine processes in the lower Columbia River: I. Along-channel water level variations, Pacific Ocean to Bonneville Dam, *Estuaries Coasts*, *38*(2), 415–433.
Jay, D. A., K. Leffler, H. L. Diefenderfer, and A. Borde (2016), Tidal-fluvial and estuarine processes in the Lower Columbia River: II: Water Level Models, Inundation, Reach Classification and Vegetation, *Estuaries Coasts*, doi:10.1007/s12237-016-0082-4, in press.
Jerolmack, D. J., and D. Mohrig (2007), Conditions for branching in depositional rivers, *Geology*, *35*(5), 463–466.
Kaiser, J. (1974), Nonrecursive digital filter design using the i_0-sinh window function, paper presented at the IEEE International Symposium on Circuits and Systems, pp. 20–23, San Francisco DA, San Francisco, Calif., April.
Kernkamp, H. W., A. Van Dam, G. S. Stelling, and E. D. de Goede (2011), Efficient scheme for the shallow water equations on unstructured grids with application to the continental shelf, *Ocean Dyn.*, *61*(8), 1175–1188.
Kim, J.-W., Z. Lu, J. W. Jones, C. Shum, H. Lee, and Y. Jia (2014), Monitoring everglades freshwater marsh water level using l-band synthetic aperture radar backscatter, *Remote Sens. Environ.*, *150*, 66–81.
Kosuth, P., J. Callède, A. Laraque, N. Filizola, J. L. Guyot, P. Seyler, J. M. Fritsch, and V. Guimarães (2009), Sea-tide effects on flows in the lower reaches of the Amazon River, *Hydrol. Process.*, *23*(22), 3141–3150.
Kukulka, T., and D. A. Jay (2003a), Impacts of Columbia River discharge on salmonid habitat: 1. A nonstationary fluvial tide model, *J. Geophys. Res.*, *108*(C9), 3293, doi:10.1029/2002JC001382.
Kukulka, T., and D. A. Jay (2003b), Impacts of Columbia River discharge on salmonid habitat: 2. Changes in shallow-water habitat, *J. Geophys. Res.*, *108*(C9), 3294, doi:10.1029/2002JC001382.
Kvale, E. P., H. W. Johnson, C. P. Sonett, A. W. Archer, and A. Zawistoski (1999), Calculating lunar retreat rates using tidal rhythmites, *J. Sediment. Res.*, *69*(6), 1154–1168.
Lamb, M. P., J. A. Nittrouer, D. Mohrig, and J. Shaw (2012), Backwater and river plume controls on scour upstream of river mouths: Implications for fluvio-deltaic morphodynamics, *J. Geophys. Res.*, *117*, F01002, doi:10.1029/2011JF002079.
Lane, E. W. (1957), *A Study of the Shape of Channels Formed by Natural Streams Flowing in Erodible Material*, US Army Eng. Division, Missouri River.
Lanzoni, S., and G. Seminara (1998), On tide propagation in convergent estuaries, *J. Geophys. Res.*, *103*(C13), 30,793–30,812.
LeBlond, P. (1978), On tidal propagation in shallow rivers, *J. Geophys. Res.*, *83*(C9), 4717–4721.
Leffler, K. E., and D. A. Jay (2009), Enhancing tidal harmonic analysis: Robust (hybrid l1/l2) solutions, *Cont. Shelf Res.*, *29*(1), 78–88.
Lemoine, R. (1948), On the positive surges in channels and on the undular jumps of low wave height, *J. La Houille Blanche*, *4*(3/4), 183–185.
Leonardi, N., A. S. Kolker, and S. Fagherazzi (2015), Interplay between river discharge and tides in a delta distributary, *Adv. Water Resour.*, *80*, 69–78.
Lighthill, J. (2001), *Waves in Fluids*, Cambridge Univ. Press, Cambridge, U. K.
Lim, Y.-H., and L. M. Lye (2004), Wavelet analysis of tide-affected low streamflows series, *J. Data Sci.*, *2*(2), 149–163.
Longuet-Higgins, M. S. (1953), Mass transport in water waves, *Philos. Trans. R. Soc. A*, *245*(903), 535–581.
Lu, S., D.-Y. Lee, J. Zheng, W. Zhang, Y. Yan, J. Shen, and C. Tong (2015), Propagation of tidal waves up in Yangtze estuary during the dry season, *J. Geophys. Res. Oceans*, *120*, 6445–6473, doi:10.1002/2014JC010414.
Lynch, D. (1982), Tidal bores, *Sci. Am.*, *247*(4), 146–157.
Maas, L. R. (1997), On the nonlinear Helmholtz response of almost-enclosed tidal basins with sloping bottoms, *J. Fluid Mech.*, *349*, 361–380.
Maas, L. R., and A. Doelman (2002), Chaotic tides, *J. Phys. Oceanogr.*, *32*(3), 870–890.
Matte, P., D. A. Jay, and E. D. Zaron (2013), Adaptation of classical tidal harmonic analysis to nonstationary tides, with application to river tides, *J. Atmos. Oceanic Technol.*, *30*(3), 569–589.
Matte, P., Y. Secretan, and J. Morin (2014), Temporal and spatial variability of tidal-fluvial dynamics in the St. Lawrence fluvial estuary: An application of nonstationary tidal harmonic analysis, *J. Geophys. Res. Oceans*, *119*, 5724–5744, doi:10.1002/2014JC009791.
Mazumder, R., and M. Arima (2005), Tidal rhythmites and their implications, *Earth Sci. Rev.*, *69*(1), 79–95.
McLusky, D., and M. Elliott (2007), Transitional waters: A new approach, semantics or just muddying the waters?, *Estuarine Coastal Shelf Sci.*, *71*(3), 359–363.
Milliman, J. D., and K. L. Farnsworth (2011), *River Discharge to the Coastal Ocean: A Global Synthesis*, Cambridge Univ. Press, Cambridge, U. K.
Moftakhari, H. R., D. A. Jay, S. A. Talke, T. Kukulka, and P. D. Bromirski (2013), A novel approach to flow estimation in tidal rivers, *Water Resour. Res.*, *49*, 4817–4832, doi:10.1002/wrcr.20363.
Moftakhari, H. R., D. A. Jay, S. A. Talke, and D. Schoellhamer (2015), Estimation of historic flows and sediment loads to San Francisco Bay, 1849–2011, *J. Hydrol.*, *529*, 1247–1261.
Mooers, C. N. (1975), Several effects of a baroclinic current on the cross-stream propagation of inertial-internal waves, *Geophys. Astrophys. Fluid Dyn.*, *6*(3), 245–275.
Münchow, A. (2000), Detiding three-dimensional velocity survey data in coastal waters, *J. Atmos. Oceanic Technol.*, *17*(5), 736–748.
Munk, W. H., B. Zetler, and G. W. Groves (1965), Tidal cusps, *Geophys. J. R. Astron. Soc.*, *10*(2), 211–219.
Munk, W., and K. Hasselmann (1964), Super-resolution of tides, in *Studies on Oceanography*, pp. 339–344, Collection of papers dedicated to Koji Hidaka, Seattle, Wash.

Munk, W. H., and D. E. Cartwright (1966), Tidal spectroscopy and prediction, *Philos. Trans. R. Soc. A*, *259*(1105), 533–581.
Nittrouer, J. A., J. Shaw, M. P. Lamb, and D. Mohrig (2012), Spatial and temporal trends for water-flow velocity and bed-material sediment transport in the lower Mississippi River, *Geol. Soc. Am. Bull.*, *124*(3–4), 400–414.
Orton, G. J., and H. G. Reading (1993), Variability of deltaic processes in terms of sediment supply, with particular emphasis on grain size, *Sedimentology*, *40*(3), 475–512.
Ozesmi, S. L., and M. E. Bauer (2002), Satellite remote sensing of wetlands, *Wetlands Ecol. Manage.*, *10*(5), 381–402.
Pagendam, D., and D. Percival (2015), Estimating freshwater flows from tidally affected hydrographic data, *Water Resour. Res.*, *51*(3), 1619–1634.
Parker, B. B. (1991a), *Tidal Hydrodynamics*, John Wiley, New York.
Parker, B. B. (1991b), The relative importance of the various nonlinear mechanisms in a wide range of tidal interactions, in *Tidal Hydrodynamics*, pp. 237–268, John Wiley, New York.
Pawlowicz, R., B. Beardsley, and S. Lentz (2002), Classical tidal harmonic analysis including error estimates in Matlab using t_tide, *Comput. Geosci.*, *28*(8), 929–937.
Peregrine, D. (1966), Calculations of the development of an undular bore, *J. Fluid Mech.*, *25*(2), 321–330.
Perroud, P. (1958), *The Propagation of Tidal Waves Into Channels of Gradually Varying Cross-Section, Ins. of Eng. Res. Ser.*, Univ. of Calif., 89, 27 pp., Berkeley, Calif.
Pethick, J. (1984), *An Introduction to Coastal Geomorphology*, Edward Arnold, London.
Pham Van, C., B. de Brye, E. Deleersnijder, A. J. F. Hoitink, M. G. Sassi, B. Spinewine, H. Hidayat, and S. Soares-Frazão (2016), Simulations of the flow in the Mahakam river-lake-delta system, Indonesia, in *Environmental Fluid Mechanics*, pp. 1–31, Springer, Netherlands.
Pham Van, C., O. Gourgue, M. G. Sassi, A. J. F. Hoitink, E. Deleersnijder, and S. Soares-Frazão (2015), Modelling fine-grained sediment transport in the Mahakam land-sea continuum, Indonesia, *J. Hydro-Environ. Res.*, doi:10.1016/j.jher.2015.04.005.
Pu, X., J. Z. Shi, G.-D. Hu, and L.-B. Xiong (2015), Circulation and mixing along the North Passage in the Changjiang River estuary, China, *J. Mar. Syst.*, *148*, 213–235.
Pugh, D. T. (1996), *Tides, Surges and Mean Sea-Level (Reprinted With Corrections)*, John Wiley, Chichester, U. K.
Rioul, O., and M. Vetterli (1991), Wavelets and signal processing, *8*, 14–38.
Romshoo, S. A. (2004), Radar remote sensing for monitoring of dynamic ecosystem processes related to biogeochemical exchanges in tropical peatlands, *Visual Geosci.*, *9*(1), 9–28.
Rossiter, J., and G. Lennon (1968), An intensive analysis of shallow water tides, *Geophys. J. Int.*, *16*(3), 275–293.
Saint-Venant, A. J. C. B. (1871), Théorie du mouvement non permanent des eaux, avec application aux crues des rivières et à l'introduction des marées dans leurs lits, *C. R. séances de l'Acad. Sci.*, *73*, 237–240.
Sassi, M. G., and A. J. F. Hoitink (2013), River flow controls on tides and tide-mean water level profiles in a tidal freshwater river, *J. Geophys. Res. Oceans*, *118*(9), 4139–4151.
Sassi, M. G., A. J. F. Hoitink, B. Vermeulen, and H. Hidayat (2011a), Discharge estimation from H-ADCP measurements in a tidal river subject to sidewall effects and a mobile bed, *Water Resour. Res.*, *47*, WO6504, doi:10.1029/2010WR009972.
Sassi, M. G., A. J. F. Hoitink, B. de Brye, B. Vermeulen, and E. Deleersnijder (2011b), Tidal impact on the division of river discharge over distributary channels in the Mahakam delta, *Ocean Dyn.*, *61*(12), 2211–2228.
Sassi, M. G., A. J. F. Hoitink, d. B. Brye, and E. Deleersnijder (2012a), Downstream hydraulic geometry of a tidally influenced river delta, *J. Geophys. Res.*, *117*, F04022, doi:10.1029/2012JF002448.
Sassi, M. G., A. J. F. Hoitink, and B. Vermeulen (2012b), Impact of sound attenuation by suspended sediment on ADCP backscatter calibrations, *Water Resour. Res.*, *48*, W09520, doi:10.1029/2012WR012008.
Sassi, M. G., A. J. F. Hoitink, B. Vermeulen, and H. Hidayat (2013a), Sediment discharge division at two tidally influenced river bifurcations, *Water Resour. Res.*, *49*, 2119–2134, doi:10.1002/wrcr.20216.
Sassi, M. G., A. J. F. Hoitink, and B. Vermeulen (2013b), Quantified turbulent diffusion of suspended sediment using acoustic Doppler current profilers, *Geophys. Res. Lett.*, *40*, 5692–5697, doi:10.1002/2013GL058299.
Savenije, H. H. G. (1992), Lagrangian solution of St. Venant's equations for alluvial estuary, *J. Hydraul. Eng.*, *118*(8), 1153–1163.
Savenije, H. H. G. (1998), Analytical expression for tidal damping in alluvial estuaries, *J. Hydraul. Eng.*, *124*(6), 615–618.
Savenije, H. H. G. (2001), A simple analytical expression to describe tidal damping or amplification, *J. Hydrol.*, *243*(3), 205–215.
Savenije, H. H. G., M. Toffolon, J. Haas, and E. J. M. Veling (2008), Analytical description of tidal dynamics in convergent estuaries, *J. Geophys. Res.*, *113*, C10025, doi:10.1029/2007JC004408.
Savoye, B., N. Babonneau, B. Dennielou, and M. Bez (2009), Geological overview of the Angola-Congo margin, the Congo deep-sea fan and its submarine valleys, *Deep Sea Res. Part II*, *56*(23), 2169–2182.
Schwartz, M. (2005), *Encyclopedia of Coastal Science*, Springer, 436 pp., Dordrecht, Netherlands.
Serre, F. (1953), Contribution à l'étude des écoulements permanents et variables dans les canaux, *La Houille Blanche*, *8*(3), 374–388.
Simon, B. (1991), Tidal hydrodynamics, in *The Species Concordance Method of Tide Prediction*, John Wiley, pp. 725–735.
Simpson, J., N. Fisher, and P. Wiles (2004), Reynolds stress and TKE production in an estuary with a tidal bore, *Estuarine Coastal Shelf Sci.*, *60*(4), 619–627, doi:10.1016/j.ecss.2004.03.006.
Slingerland, R., and N. D. Smith (2004), River avulsions and their deposits, *Annu. Rev. Earth Planet. Sci.*, *32*, 257–285.
Souza, A., and A. Hill (2006), Tidal dynamics in channels: Single channels, *J. Geophys. Res.*, *111*, C09037, doi:10.1029/2006JC003469.
Sun, G., K. Ranson, V. Kharuk, and K. Kovacs (2003), Validation of surface height from shuttle radar topography mission using shuttle laser altimeter, *Remote Sens. Environ.*, *88*(4), 401–411.
Syvitski, J. P., et al. (2009), Sinking deltas due to human activities, *Nat. Geosci.*, *2*(10), 681–686.
Talke, S. A., and D. A. Jay (2013), Nineteenth century North American and Pacific tidal data: Lost or just forgotten?, *J. Coastal Res.*, *29*(6a), 118–127.
Te Chow, V. (1959), *Open Channel Hydraulics*, 660 pp., McGraw-Hill Book Company, Inc., New York.
Thomson, R. E., and W. J. Emery (2014), *Data Analysis Methods in Physical Oceanography*, Newnes, Boston.
Toffolon, M., and H. H. Savenije (2011), Revisiting linearized one-dimensional tidal propagation, *J. Geophys. Res.*, *116*, C07007, doi:10.1029/2010JC006616.
Torrence, C., and G. P. Compo (1998), A practical guide to wavelet analysis, *Bull. Am. Meteorol. Soc.*, *79*(1), 61–78.
Twigt, D. J., E. D. De Goede, F. Zijl, D. Schwanenberg, and A. Y. Chiu (2009), Coupled 1D–3D hydrodynamic modelling, with application to the Pearl River delta, *Ocean Dyn.*, *59*(6), 1077–1093.
Uncles, R., J. Stephens, and R. Smith (2002), The dependence of estuarine turbidity on tidal intrusion length, tidal range and residence time, *Cont. Shelf Res.*, *22*(11), 1835–1856.

Uncles, R. J., J. A. Stephens, and M. L. Barton (1991), The nature of near-bed currents in the upper reaches of an estuary, in *Estuaries and Coasts: Spatial and Temporal Intercomparisons*, pp. 43–47.

Vellinga, N. E., A. J. F. Hoitink, M. van der Vegt, W. Zhang, and P. Hoekstra (2014), Human impacts on tides overwhelm the effect of sea level rise on extreme water levels in the Rhine–Meuse delta, *Coastal Eng.*, *90*, 40–50.

Vennell, R., and R. Beatson (2006), Moving vessel acoustic doppler current profiler measurement of tidal stream function using radial basis functions, *J. Geophys. Res.*, *111*(C9).

Vermeulen, B., A. J. F. Hoitink, and M. Sassi (2011), Coupled ADCPs can yield complete Reynolds stress tensor profiles in geophysical surface flows, *Geophys. Res. Lett.*, *38*, L06406, doi:10.1029/2011GL046684.

Vermeulen, B., A. J. F. Hoitink, and M. G. Sassi (2013), On the use of horizontal acoustic Doppler profilers for continuous bed shear stress monitoring, *Int. J. Sediment Res.*, *28*(2), 260–268.

Vermeulen, B., M. G. Sassi, and A. J. F. Hoitink (2014), Improved flow velocity estimates from moving-boat ADCP measurements, *Water Resour. Res.*, *50*, 4186–4196, doi:10.1002/2013WR015152.

Vetterli, M., and C. Herley (1992), Wavelets and filter banks: Theory and design, *IEEE Trans. Signal Process.*, *40*(9), 2207–2232.

White, M. A., J. C. Schmidt, and D. J. Topping (2005), Application of wavelet analysis for monitoring the hydrologic effects of dam operation: Glen Canyon Dam and the Colorado River at Lees Ferry, Arizona, *River Res. Appl.*, *21*(5), 551–565.

Wiele, S. M., and J. D. Smith (1996), A reach-averaged model of diurnal discharge wave propagation down the Colorado River through the Grand Canyon, *Water Resour. Res.*, *32*(5), 1375–1386.

Wolanski, E., D. Williams, S. Spagnol, and H. Chanson (2004), Undular tidal bore dynamics in the Daly Estuary, Northern Australia, *Estuarine Coastal Shelf Sci.*, *60*(4), 629–636, doi:10.1016/j.ecss.2004.03.001.

Xue, P., C. Chen, P. Ding, R. C. Beardsley, H. Lin, J. Ge, and Y. Kong (2009), Saltwater intrusion into the Changjiang River: A model-guided mechanism study, *J. Geophys. Res.*, *114*, C02006, doi:10.1029/2008JC004831.

Young, P. C., D. J. Pedregal, and W. Tych (1999), Dynamic harmonic regression, *J. Forecasting*, *18*(6), 369–394.

Zaron, E. D., and D. A. Jay (2014), An analysis of secular change in tides at open-ocean sites in the Pacific, *J. Phys. Oceanogr.*, *44*(7), 1704–1726.

Zhang, E. F., H. H. G. Savenije, S. L. Chen, and X. H. Mao (2012a), An analytical solution for tidal propagation in the Yangtze Estuary, China, *Hydrol. Earth Syst. Sci.*, *16*(9), 3327–3339.

Zhang, W., Y. Yan, J. Zheng, L. Li, X. Dong, and H. Cai (2009), Temporal and spatial variability of annual extreme water level in the Pearl River Delta region, China, *Global Planet. Change*, *69*(1), 35–47.

Zhang, W., H. Feng, J. Zheng, A. J. F. Hoitink, M. Van Der Vegt, Y. Zhu, and H. Cai (2012b), Numerical simulation and analysis of saltwater intrusion lengths in the Pearl River Delta, China, *J. Coastal Res.*, *29*(2), 372–382.

Zhang, W., J. Du, J. Zheng, X. Wei, and Y. Zhu (2013), Redistribution of the suspended sediment at the apex bifurcation in the Pearl River Network, South China, *J. Coastal Res.*, *30*(1), 170–182.

Zolezzi, G., A. Bellin, M. C. Bruno, B. Maiolini, and A. Siviglia (2009), Assessing hydrological alterations at multiple temporal scales: Adige River, Italy, *Water Resour. Res.*, *45*, W12421, doi:10.1029/2008WR007266.